Lithos 212–215 (2015) 428–442

Contents lists available at ScienceDirect

Lithos

journal homepage: www.elsevier.com/locate/lithos

Zircon U–Pb dating, geochemistry and Sr–Nd–Pb–Hf isotopes of the Wajilitag alkali mafic dikes, and associated diorite and syenitic rocks: Implications for magmatic evolution of the Tarim large igneous province

Si-Yuan Zou [a], Zi-Long Li [a,*], Biao Song [b], Richard E. Ernst [c], Yin-Qi Li [a], Zhong-Yuan Ren [d], Shu-Feng Yang [a], Han-Lin Chen [a], Yi-Gang Xu [d], Xie-Yan Song [e]

[a] Department of Earth Sciences, Zhejiang University, Hangzhou 310027, PR China
[b] Beijing SHRIMP Center, Institute of Geology, Chinese Academy of Geological Sciences, Beijing 100037, PR China
[c] Department of Earth Sciences, Carleton University, Ottawa K1S 5B6, Canada
[d] State Key Laboratory of Isotope Geochemistry, Guangzhou Institute of Geochemistry, China Academy of Sciences, Guangzhou 510640, PR China
[e] Institute of Geochemistry, China Academy of Sciences, Guiyang 550002, PR China

ARTICLE INFO

Article history:
Received 10 November 2013
Accepted 8 September 2014
Available online 21 September 2014

Keywords:
Zircon U–Pb dating
Sr–Nd–Pb–Hf isotopes
Magma source
Magmatic evolution
Wajilitag complex
Tarim large igneous province

ABSTRACT

The Early Permian Tarim large igneous province (Tarim LIP) consists mainly of basaltic lavas, mafic–ultramafic intrusions including dikes and, syenite bodies in the Tarim Basin, NW China. A major unit of the Tarim LIP, the Wajilitag intrusive complex, consists of olivine pyroxenite, clinopyroxenite and gabbro units (from bottom to top), diorite and syenite rocks occurred in the upper part of the complex and alkali mafic dikes intrude the clinopyroxenite phase. Here we report the zircon U–Pb age and Hf isotopes, geochemical characteristics and Sr–Nd–Pb isotopic data of the alkali mafic dikes, and diorite, aegirine–nepheline syenite and syenite porphyry units in the Wajilitag intrusive complex. Zircons from the diorite and alkali mafic rocks yield concordant crystallization ages of 275.2 ± 1.2 Ma and 281.4 ± 1.7 Ma, respectively. The diorite and syenitic rocks in Wajilitag area have a narrow range of SiO_2 contents (51.9–57.3 wt.%), and are enriched in total alkalis ($Na_2O + K_2O$ = 8.3–14.3 wt.%), among which the aegirine–nepheline syenite and syenite porphyry have the geochemical affinity of A-type granites. The alkali mafic rocks and syenitic rocks have high Al_2O_3 (19.4–21.1 wt.%), Zr, Hf, Ba contents, total rare earth element abundances and LREE/HREE ratios and low Mg# value, K, P and Ti contents. Diorites have lower Al_2O_3 contents, total REE abundances and LREE/HREE ratios and higher Mg# values than the alkali mafic rocks and syenitic rocks. The diorites and syenitic rocks have low initial $^{87}Sr/^{86}Sr$ ratios (0.7034–0.7046), and high $\varepsilon Nd(t)$ values (0.1–4.1) and zircon $\varepsilon Hf(t)$ values (−0.9–4.4). All the diorites and syenitic rocks show the $^{206}Pb/^{204}Pb$ ratios ranging of 18.0–19.5, $^{207}Pb/^{204}Pb$ of 15.4–15.6 and $^{208}Pb/^{204}Pb$ of 38.0–39.9. Sr–Nd isotopic ratios indicate a FOZO-like mantle source for the diorite and syenitic rocks, similar to that of the mafic–ultramafic rocks in the Wajilitag complex. In contrast, zircon Hf isotopes of basalt and syenite elsewhere in the Tarim LIP indicate a FOZO-like component may also contribute to Tarim LIP magmatism. Geochemical and Sr–Nd–Pb–Hf isotopic features reflect that diorites and syenitic rocks are probably derived from a FOZO-like mantle source, consistent with a plume mantle origin and then underwent crystal fractionation process.

1. Introduction

The Tarim large igneous province (Tarim LIP), formed during the early Permian, is located in the Tarim Basin, the largest basin in China (Li et al., 2011; Z.L. Li et al., 2012; Yang et al., 2006, 2007; Yu, 2009; Zhang et al., 2008), and is mainly composed of basalts and numerous intrusions. It is comparable to the Siberian Traps and Emeishan large igneous province occurred in the Eurasian continent during the Permian. The Tarim basalts typically formed earlier than the Tarim intrusive rocks in a within-plate setting (X. Yu et al., 2011; Zhou et al., 2009).

The mid-ocean ridge basalts (MORB) and ocean island basalts (OIB) are considered as the result of mixing between several end-members, such as DMM (depleted MORB mantle), HIMU (high μ = high U/Pb), EMI (enriched mantle with low $\varepsilon Nd(t)$ and $^{206}Pb/^{204}Pb$, and intermediate initial $^{87}Sr/^{86}Sr$), EMII (enriched mantle with intermediate $\varepsilon Nd(t)$, and high $^{206}Pb/^{204}Pb$ and initial $^{87}Sr/^{86}Sr$) and FOZO (Focus Zone) (Hart, 1988; Hart et al., 1992; Hofmann, 2003; Saal et al., 2005; Stracke et al., 2005; Tackley, 2007; Willbold and Stracke, 2010; Zindler and Hart, 1986). Previous studies revealed Keping basalts are derived from an OIB-like (EMII) components whereas the intrusive rocks originated from a mixing between the DDM and EMII end-member

* Corresponding author at: Department of Earth Sciences, Zhejiang University, 38 Zheda Road, Hangzhou 310027, PR China. Tel./fax: +86 571 87951580.
E-mail address: zilongli@zju.edu.cn (Z.-L. Li).

http://dx.doi.org/10.1016/j.lithos.2014.09.005
0024-4937/

interpreted to represent the interaction between OIB-like asthenospheric (plume) mantle and subcontinental lithospheric mantle, based on their whole-rock geochemistry, Sr–Nd–Pb–Hf isotopes and PGE values (Li et al., 2011; Y.Q. Li et al., 2010, 2012; Z.L. Li et al., 2012; Yang et al., 2007; Zhang et al., 2008; C.L. Zhang et al., 2010). While geochemistry and Sr–Nd isotopes for the mafic to ultramafic igneous rocks in the Xiaohaizi and Wajilitag areas of Bachu County have been studied well, the newly discovered alkali mafic dikes (mainly refers to alkali diabase) and diorite as well as syenitic and syenitic porphyry units of the Wajilitag complex should be further studied.

Alkali mafic dike, diorite and syenitic rocks have been identified as important units of some large intrusions in some LIPs (Shellnutt et al., 2011; Song et al., 2008; Xu et al., 2008; Zhou et al., 2006). The various diabase and bimodal dikes intruded into the strata and intrusions and always had great significance to restrict the relationship among different rock types (Li et al., 2011; Shellnutt et al., 2012; Yang et al., 2007). For instance, diorite can often appear with gabbro in the intrusions and makes a vital contribution to ore deposit mineralization.

The Wajilitag complex (also known as the Bachu intrusions; Zhang et al., 2008) is a key intrusion in Tarim LIP. This paper presents new geochemistry, Sr–Nd–Pb–Hf isotopic data and zircon U–Pb dating of the new discovered diorite, nepheline-bearing syenite and syenite porphyry units in the upper part of the Wajilitag complex and the alkali mafic dikes cutting these units. These data will be integrated with published data for the mafic–ultramafic portions of the Wajilitag complex to provide a more complete interpretation of the magmatic source(s) and evolutionary history of this important Wajilitag complex of the Tarim LIP and with implications for the Tarim LIP as a whole.

2. Geological background

2.1. Regional geology

The Tarim Basin, surrounded by the Tianshan, Kunlun and Altun Mountains in the northwestern China (Fig. 1a, b), is underlain by a Precambrian crystalline basement and consists of Phanerozoic sedimentary strata ranging in age from Ordovician to Neogene (Chen et al., 1997a,b; Jia, 1997; Jia et al., 1995; Jiang et al., 2004; Z.L. Li et al., 2012; Yang et al., 2006, 2007; X. Yu et al., 2011; Zhang et al., 2003; C.L. Zhang et al., 2013; D.Y. Zhang et al., 2013; Zhou et al., 2009). The Permian igneous rocks of the Tarim Basin have been well studied through a number of field geological investigations, drill core records, geophysical investigation and geochemical and geochronological studies (Borisenko et al., 2006; Cao et al., 2014; Chen et al., 1997a,b, 2010; Jia, 1997; Jia et al., 1995; Jiang et al., 2004; Li, 2013; Y.Q. Li et al., 2010; Li et al., 2011; Y.Q. Li et al., 2012; Z.L. Li et al., 2012; Tian et al., 2010; Wei et al., 2014; Xu et al., 2014; Yang et al., 2006, 2007; Yu et al., 2009; J.C. Yu et al., 2011; X. Yu et al., 2011; Yu et al., 2012; Zhang et al., 2003, 2008; C.L. Zhang et al., 2010; D.Y. Zhang et al., 2010; Y.T. Zhang et al., 2010; D.Y. Zhang et al., 2013; Zhou et al., 2009; Zou et al., 2013). The Permian strata in the Tarim Basin are composed of volcanic sedimentary and sedimentary sequences, including limestones, sandstones, siltstones and basaltic lava. As the main phase of the Tarim LIP, the continental flood basalts are distributed over an area of more than 250,000 km^2 (Yang et al., 2007). In addition, the mafic–ultramafic intrusions, kimberlitic intrusions, syenitic bodies, mafic and bimodal dikes discovered in Bachu area are also the parts of the Tarim LIP (Cao et al., 2014; Li et al., 2011; Y.Q. Li et al., 2012; Wei and Xu, 2011; Yang et al., 2006, 2007; Yu et al., 2009; Zhang et al., 2008; D.Y. Zhang et al., 2013; Zhou et al., 2009). Some researchers suggested that the early Permian igneous event was probably caused by a Permian mantle plume upwelling under the Tarim Block (Li, 2013; Li et al., 2008; Z.L. Li et al., 2012; Zhang et al., 2008).

2.2. The Wajilitag complex

The intrusive complex is located in Wajilitag area of the southeastern Bachu County in the western Tarim Basin (Fig. 1b), and has a layered structure with an outcropping area of ca. 15 km^2 (Fig. 1c). It has been previously referred to as the Bachu layered intrusive complex (Zhang et al., 2008), but herein is referred to as the Wajilitag ntrusive complex. The complex consists of a sill-like mafic–ultramafic layered intrusion, syenitic bodies, mafic dike swarms and bimodal dikes, and intruded into the Silurian–Devonian sedimentary rocks with contact zones dipping 20–40° toward the interior of the complex. The complex has a thickness of ca. 100–300 m and extends over an area of ca. 15 km^2 (Cao et al., 2014; Y.Q. Li et al., 2012). The intrusion consists of a sequence of olivine pyroxenite, clinopyroxenite and gabbro from bottom to top in the intrusion (Cao et al., 2014; Zhang et al., 2008). The Fe–Ti oxide deposit is mainly located in the clinopyroxenite unit, and contains 100 million tons of ore reserves with ca. 20 wt.% FeO_T, 7 wt.% TiO_2 and 0.14 wt.% V_2O_5 (Gao, 2007). Apart from the layered intrusion, there are syenitic and diorite bodies outcropping above the mafic–ultramafic intrusion with a sharp contact. Numerous mafic and bimodal dikes intruded into the mafic–ultramafic layered intrusion and the host upper Devonian sedimentary rocks; these dikes have variable trends (C.L. Zhang et al., 2010). A similar situation applies to the mafic dikes and bimodal dikes that crop out around the neighboring Xiaohaizi intrusive complex (Yang et al., 2007). Moreover, the Wajilitag complex also has some transitional rock types (e.g., plagioclase-bearing pyroxenite, olivine gabbro, hornblende-bearing syenite, aegirine–nepheline syenite, quartz syenite). On the basis of the geochemical and geochronological data of the intrusive rocks, Zhang et al. (2008) suggested that the emplacement age of the Wajilitag (Bachu) complex was ca. 275 Ma and that it was a product of a Permian mantle plume emplaced at the base of the lithosphere below the Tarim Basin. Yang et al. (2007) proposed that the syenitic porphyry in the Xiaohaizi area formed in a within-plate environment at ca. 277 Ma and was derived from differentiation of mantle derived melts; and Yu et al. (2009) reported the formation of mafic–ultramafic igneous rocks in the same area being genetically related to a mantle plume rising under Tarim Basin. Building on the previous studies on the mafic–ultramafic layered intrusion, these additional mafic dikes and quartz syenite all belonging to the Wajilitag intrusive complex, we analyzed the diorite and aegirine–nepheline syenitic bodies, alkali mafic dikes and bimodal dikes which intruded into the clinopyroxenite and syenite porphyry (Fig. 2a, b, c).

3. Petrography of the Wajilitag alkali mafic diked rocks, diorite and syenitic rocks

The rocks of this study are distributed in the Wajilitag area (Fig. 1c) and associated with the mafic–ultramafic rocks of the Wajilitag complex. The newly characterized units of this study include alkali diabase, syenitic porphyry, aegirine–nepheline syenite and diorite.

The aegirine–nepheline syenite consists of orthoclase (60–70%), nepheline (5–10%), aegirine (20%) and biotite (1–5%) as well as apatite, zircon and magnetite (Fig. 2d, e).

The diorite is mainly composed of plagioclase (60–70%), hornblende (10–15%), brown biotite (8–10%), augite (5–10%), opaque minerals (5–10%) and perthite (5%) with accessory zircon and apatite. Plagioclase exhibits characteristic zoning and twinning, and some plagioclase grains are surrounded by perthite. In addition, some hornblende grains are replaced by biotite (Fig. 2f).

The alkali mafic dike has a microporphyritic texture (Fig. 2g) with phenocrysts of plagioclase (30%) which display carlsbad–albite compound twining and compositional zoning. In the matrix, aegirine–augite (30–40%) and plagioclase (30–40%) exhibit a diabasic texture (Fig. 2h).

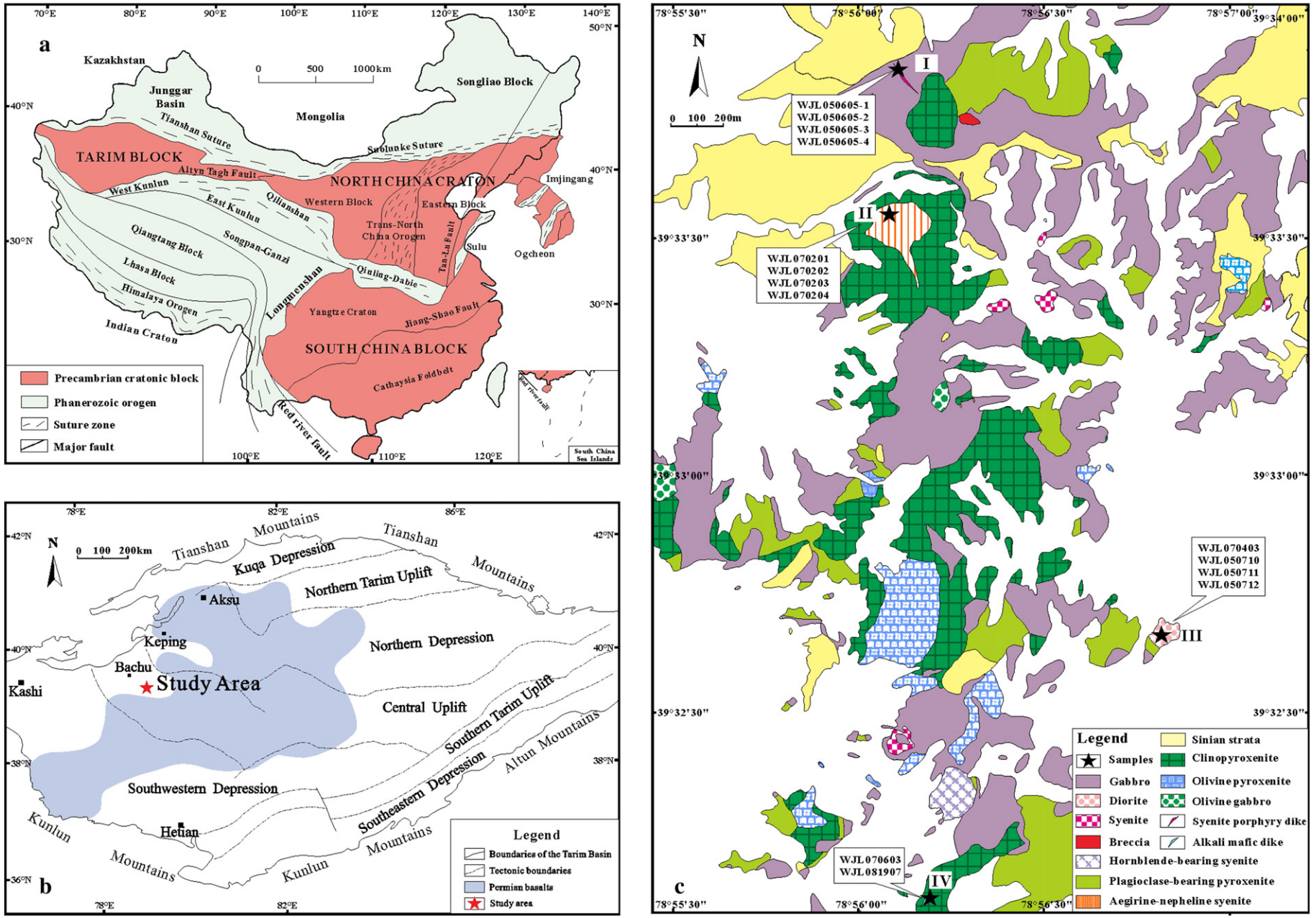

Fig. 1. Geotectonic units of (a) China (referred to Li, 2013) and (b) Tarim Basin (referred to Li et al., 2008) and (c) lithological sketch map of the Wajilitag area (the syenite porphyry, aegirine–nepheline syenite, diorite and alkali mafic rock samples are located in the areas of I, II, III and IV, respectively).

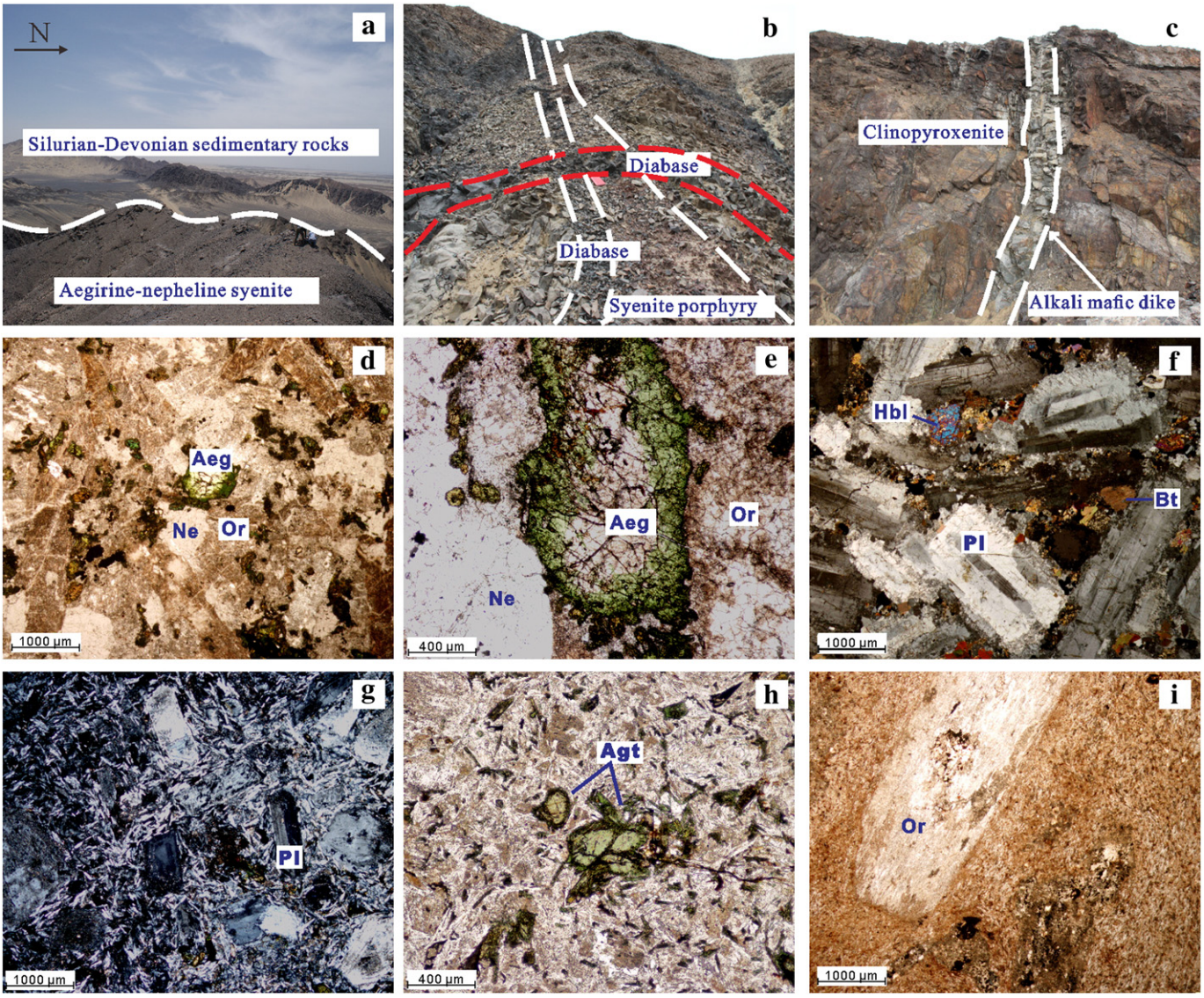

Fig. 2. Field photos and microphotos of the samples in Wajilitag area: (a) aegirine–nepheline syenite bodies intruding into the Silurian–Devonian sedimentary rocks; (b) bimodal diabase and syenite porphyry dikes; (c) alkali mafic dike intruded into the clinopyroxenite; (d) and (e) petrography of aegirine-nepheline syenite with minerals of aegirine, nepheline and orthoclase; (f) zoned and subhedral structure of plagioclase in diorite; (g) and (h) large plagioclase phenocryst and aegirine–augite in alkali diabase, and (i) microcrystalline texture in syenite porphyry. Mineral abbreviations in the microphotos: aegirine (Aeg), nepheline (Ne), orthoclase (Or), hornblende (Hbl), biotite (Bt), plagioclase (Pl), and aegirine–augite (Agt).

The syenite porphyry has a microcrystalline texture typically with phenocrysts of orthoclase (20–30%). Orthoclase phenocrysts display corroded rims (Fig. 2i).

4. Analytical methods

4.1. Zircon U–Pb dating and Hf isotope analyses

The samples of the diorite (WJL050710) and alkali mafic rock (WJL081907) were selected for zircon U–Pb dating. Zircon grains were first separated by conventional magnetic and density techniques, and then selected by hand-picking under a binocular microscope. Representative zircon grains along with TEMORA standard (417 Ma) were embedded in epoxy resin and polished to expose the crystals for dating. Transmitted and reflected light micrographs as well as cathodoluminescence (CL) images were obtained for the polished zircon grains before U–Pb isotope analyses in order to reveal their internal structure and external morphology and guide the selection of potential analytical spots. The CL images were made using a HITACHI S3000-N Scanning electron microscope at Beijing SHRIMP Center, Chinese Academy of Geological Sciences, Beijing.

Zircon from the diorite was dated in situ on an ArF-excimer (193-nm wavelength) laser ablation multiple-collector inductively coupled plasma mass spectrometer (LA-ICPMS) at the Tianjin Institute of Geology and Mineral Resources, China Geological Survey. The ICP-MS used was a Neptune made by Thermo Fisher, and the UP193-FX ArF laser ablation system (ESI Company) was used for the laser ablation experiments. The instrumental conditions and analytical processes were similar to those described by Hou et al. (2009). U and Pb concentrations were calibrated by using TEMORA and GJ-1 as external standards (Jackson et al., 2004). $^{207}Pb/^{206}Pb$, $^{206}Pb/^{238}U$, $^{207}Pb/^{235}U$, and $^{208}Pb/^{232}Th$ ratios, calculated using the ICPMSDataCal program (Liu et al., 2009) and the Isoplot program (Ludwig, 2003), were corrected for both instrumental mass bias and elemental and isotopic fractionation by using standard glass NIST612 as an external standard. The age data are in Supplementary Table 1.

In addition, in situ U–Th–Pb isotopic analyses of zircons from the alkali mafic dikes were carried out using the sensitive high resolution ion micro probe (SHRIMP IIe-MC) at Beijing SHRIMP Center, Chinese

Table 1
Geochronological data of Permian intrusive rocks in Bachu area.

Location	Rock units	Rock types	Ages (Ma)	Methods	References
Xiaohaizi	Dike	Diabase	272 ± 6	Zircon LA-ICP-MS	Li et al. (2007)
Xiaohaizi	Intrusive complex	Syenite	277.7 ± 1.3	$^{40}Ar/^{39}Ar$	Yang et al. (1996)
Xiaohaizi	Intrusive complex	Syenite	277 ± 4	Zircon SHRIMP	Yang et al. (2006)
Xiaohaizi	Intrusive complex	Hornblende syenite	279.7 ± 2.0	Zircon SIMS	Wei and Xu (2011)
Xiaohaizi	Intrusive complex	Syenite	281 ± 4	Zircon LA-ICP-MS	Li et al. (2007)
Xiaohaizi	Intrusive complex	Syenite	282 ± 3	Zircon LA-ICP-MS	Li et al. (2007)
Xiaohaizi	Intrusive complex	Gabbro	283.1 ± 3.2	Zircon LA-ICP-MS	Zhang et al. (2009)
Xiaohaizi	Bimodal dike	Quartz syenite	284.3 ± 2.8	Zircon SHRIMP	Li et al. (2011)
Wajilitag	Intrusive complex	Quartz syenite	273.7 ± 1.5	Zircon SHRIMP	Zhang et al. (2008)
Wajilitag	Intrusive complex	Diorite	275.2 ± 1.2	Zircon LA-ICP-MS	This study
Wajilitag	Dike	Alkali mafic rock	281.4 ± 1.7	Zircon SHRIMP	This study
Wajilitag	Intrusive complex	Granodiorite	295.9 ± 2.1	Zircon LA-ICP-MS	Zhang et al. (2009)
Wajilitag	Kimberlic pipe	Kimberlitic rock	299.8 ± 4.3	Perovskite SHRIMP	Zhang et al. (2013a)
Wajilitag	Kimberlic dike	Kimberlitic rock	300.5 ± 4.4	Baddeleyite SHRIMP	Zhang et al. (2013a)
Wajilitag	Kimberlic dike	Kimberlitic rock	300.8 ± 4.7	Baddeleyite SHRIMP	Zhang et al. (2013a)

Academy of Geological Sciences, Beijing. The analytical procedures are after Song et al. (2002) and Williams (1998). Primary beam size was 25 μm, and each site was rastered for 150–200 s prior to the analyses. Between each three analyses, a standard zircon (TEMORA) was analyzed for calibration. The common lead correction was referred to the measured ^{204}Pb abundances. Data processing was performed using the SQUID and ISOPLOT programs (Ludwig, 2003). Errors for individual analyses are quoted at 2σ (two standard deviation) with 95% confidence level. The data of the ages are listed in Supplementary Table 2.

Hf isotope data was obtained using a Neptune Plus multiple-collector inductively coupled plasma mass spectrometer with RESOlution M-50-LR laser ablation (ArF-excimer 193-nm wavelength) at the Guangzhou Institute of Geochemistry of Chinese Academy of Sciences. The Hf isotopic analysis spots coincided with the U-Pb dating spots, and Penglai zircons were selected as reference material (X.H. Li et al., 2010) with the precision being 0.282882 ± 0.000006 (2 s, N = 56). The analytical procedures and principles used were similar to those described by Wu et al. (2006). In the experiment, helium was used as the abrasion material carrier gas, and the diameter of the laser beam spot is 33 μm with energy of 80 mJ and repeat frequency of 8 Hz. The Hf isotopic results are listed in Supplementary Table 3.

4.2. Electron microprobe analyses

Major element compositions of plagioclase and biotite in the diorite sample (Wjl070403) were measured by the electron probe micro analyzer (EPMA, JEOL JXA-8100) at the Second Institute of Oceanography, State Oceanic Administrator, Hangzhou, China. Quantitative analysis followed the analytical procedure of Iizuka et al. (2005), using a 5 μm defocused beam with a beam current of 20 nA and acceleration voltage of 15 kV. The measured X-ray intensities were corrected by the ZAF method using the standard analysis of synthetic standard minerals with various diffracting crystals. The relative standard deviations (RSD) for Si, Na and K were less than 1 wt.%, and for other elements was less than 0.5 wt.%. Detection limits were less than 500 ppm for all elements based on 2σ of standard calibration. Concentrations of ferrous and ferric iron were calculated using stoichiometry and charge balance. More detailed information for this method is provided in Y.Q. Li et al. (2012), and the representative compositional data are given in Supplementary Tables 4 and 5.

4.3. Major and trace elemental analyses

Thirteen samples of alkali diabase, diorite and syenitic rocks were selected for major and trace elemental analyses. Major elements were analyzed by X-ray fluorescence (XRF) (Rigaku 3270E) at the Guangzhou Institute of Geochemistry, Chinese Academy of Sciences. Analytical precision was generally better than 2% for most oxides and better than 1% for SiO_2. Trace element data were obtained at Harvard University of USA by inductively coupled plasma mass spectrometer (ICP-MS) using the analytical procedure of Bézos et al. (2009). ^{72}Ge, ^{103}Rh, ^{115}In, ^{169}Tm and ^{209}Bi were selected as internal standard normalization and international standards BHVO-2, BCR-2, AGV-1, DNC-1, W-2 and JB-2 were chosen as calibration standards for calculation of element concentrations of the measured samples. The analytical precision was better than 5% for trace elements. The major and trace elemental data from 13 samples and international standard materials in this paper are listed in Table 2 and Appendix 1.

4.4. Sr–Nd–Pb isotopic analyses

The samples selected for Sr–Nd–Pb isotopic analyses were ground with an agate mill, and powders were spiked with mixed isotope tracers, dissolved in Teflon capsules with HF + HNO_3 acid, and separated by conventional cation-exchange techniques with diluted HBr as an eluant. The isotopic measurements were performed on a Finnigan MAT-262 mass-spectrometer at the Institute of Geology and Geophysics, Chinese Academy of Sciences. The mass fractionation corrections for Sr and Nd isotopic ratios were based on $^{86}Sr/^{88}Sr = 0.1194$ and $^{146}Nd/^{144}Nd = 0.7219$. Repeat analyses yielded a $^{87}Sr/^{86}Sr$ ratio of 0.710252 ± 0.000025 for the NBS-987 Sr standard and a $^{143}Nd/^{144}Nd$ ratio of 0.512118 ± 0.000012 for the JNdi-1 Nd standard. Repeat analyses yielded $^{204}Pb/^{206}Pb = 0.05897 \pm 0.00015$, $^{207}Pb/^{206}Pb = 0.91445 \pm 0.00080$, $^{208}Pb/^{206}Pb = 2.16170 \pm 0.00180$ for NBS981 Pb standard. Detailed descriptions of the analytical techniques are given by Wei et al. (2004) and Zeng et al. (2014). All analytical results in this study are presented in Tables 3 and 4.

5. Results

5.1. Zircon U–Pb age and Hf isotopic results of the Wajilitag diorite

Zircon grains from the sample (wjl050710) of the diorite are mostly euhedral, transparent, colorless, and 100–300 μm in length, with length-to-width ratios of 1.5–3. Under CL images (Fig. 3), most crystals have euhedral concentric zoning, consistent with a magmatic origin (Belousova et al., 2002). Analyses were conducted on 29 zircon grains, and the isotopic ratios and calculated ages are listed in Table 2. In the $^{206}Pb/^{238}U$-$^{207}Pb/^{235}U$ concordia plot (Fig. 4), the 29 analyses are concordant within error, and yield a weighted mean $^{206}Pb/^{238}U$ age of 275.2 ± 1.2 Ma (2σ, MSWD = 0.30).

Zircons from the alkali mafic rock (WJL081907) are euhedral but partly fragmented. Six transparent, colorless and intact grains were selected for analyses, and the isotopic ratios and calculated ages are listed in Supplementary Table 2. In the $^{206}Pb/^{238}U$ vs.$^{207}Pb/^{235}U$ concordia plot

Table 2
Major, trace and rare earth elements of the Wajilitag alkali mafic rock, diorite and syenitic rocks.

Sample no.	WJL070201	WJL070202	WJL070203	WJL070204	WJL050605-1	WJL050605-2	WJL050605-3	WJL050605-4	WJL050710	WJL050711	WJL050712	WJL070603	WJL081907
Rock type	Aegirine–nepheline syenite				Syenite porphyry				Diorite			Alkali mafic rock	
SiO_2	52.82	52.14	51.93	53.97	55.39	54.61	55.05	54.74	55.61	57.27	54.52	56.71	57.05
TiO_2	1.11	0.88	0.69	0.66	0.75	0.74	0.77	0.73	1.73	1.40	1.74	0.41	0.45
Al_2O_3	19.47	19.81	20.15	21.12	19.73	19.36	19.54	19.40	16.37	17.03	17.10	20.48	20.59
Fe_2O_{3T}	5.76	5.44	6.60	4.41	4.75	5.04	4.32	5.88	8.98	7.04	8.61	3.22	3.26
MnO	0.22	0.19	0.16	0.15	0.26	0.25	0.20	0.19	0.15	0.10	0.14	0.19	0.18
MgO	1.09	0.91	0.74	0.67	0.61	0.60	0.65	0.49	2.87	2.21	2.94	0.34	0.60
CaO	3.79	3.42	2.58	2.24	1.92	2.44	2.08	1.90	4.42	3.88	5.04	1.65	1.66
Na_2O	9.06	9.26	9.42	8.91	5.95	6.74	7.17	6.32	5.14	5.57	5.08	10.50	10.18
K_2O	4.16	4.55	4.85	5.11	5.73	4.74	4.38	5.44	3.38	4.09	3.26	3.83	3.81
P_2O_5	0.25	0.20	0.13	0.11	0.19	0.18	0.19	0.19	0.48	0.35	0.63	0.05	0.06
LOI	1.98	2.78	2.33	2.23	4.45	5.09	5.51	4.44	0.42	0.60	0.47	2.15	1.68
Total (wt%)	99.73	99.59	99.59	99.57	99.73	99.79	99.84	99.72	99.54	99.54	99.54	99.53	99.53
Sc (ppm)	1.24	1.02	0.92	-0.01	0.34	0.48	0.67	0.33	6.04	4.74	5.37	0.60	0.45
V	46.96	41.50	34.48	28.92	15.39	18.90	18.26	19.41	87.39	71.51	85.11	25.65	24.85
Cr	194.93	8.43	13.28	119.05	179.57	5.52	159.06	9.15	32.33	28.41	14.62	2.33	1.77
Co	8.12	6.66	6.65	5.07	3.84	3.75	3.67	4.19	18.73	13.04	19.20	17.94	21.14
Ni	17.72	7.67	10.02	10.92	13.25	4.34	12.62	5.79	32.18	24.89	25.16	2.64	2.25
Cu	73.38	38.10	49.77	56.26	60.04	70.12	49.69	68.70	336.32	172.90	186.07	35.98	25.89
Zn	203.73	211.52	133.20	120.83	354.04	669.82	124.72	378.48	373.95	204.26	256.21	161.76	133.18
Ga	31.69	31.40	32.89	35.19	33.95	33.94	35.79	31.60	25.65	25.48	25.83	42.63	41.66
Rb	90.59	96.87	129.78	140.97	83.31	66.70	55.49	78.24	40.68	64.23	26.24	105.99	97.93
Sr	2854.85	2725.81	1954.68	1698.18	1917.59	1227.72	905.95	1166.63	700.79	556.59	940.16	1425.49	1922.12
Y	56.57	51.70	31.65	22.01	47.29	46.89	59.35	50.10	27.07	22.49	26.75	37.56	40.23
Zr	1152.82	917.28	626.62	699.18	1533.04	1590.82	1575.53	1176.42	182.54	194.93	154.10	1431.08	1430.87
Nb	242.15	189.88	128.03	121.58	315.31	309.26	376.77	307.43	96.15	78.00	88.78	271.65	280.27
Cs	2.13	1.39	1.18	1.10	2.14	3.90	3.52	3.99	0.81	0.99	0.58	1.00	1.16
Ba	2950.50	2730.67	1565.03	1566.48	1624.53	1808.58	1179.81	2428.09	1078.06	1227.11	1496.51	2043.82	2375.55
La	181.64	208.76	138.53	86.16	135.16	147.83	156.49	151.25	56.41	49.93	54.79	182.59	176.03
Ce	322.60	347.61	218.45	146.47	253.24	260.93	277.02	258.52	128.04	103.37	133.23	277.74	282.22
Pr	29.50	31.27	18.56	12.83	21.10	23.21	24.48	23.04	12.63	10.58	12.90	21.53	20.30
Nd	95.76	97.94	57.12	40.01	66.95	73.33	76.91	71.88	46.26	37.44	47.70	63.32	57.45
Sm	14.86	13.96	8.08	5.91	10.42	10.88	12.80	10.91	8.33	6.51	8.56	8.32	7.62
Eu	4.34	3.97	2.30	1.71	3.00	3.04	3.83	3.18	2.45	2.00	2.68	2.54	2.58
Gd	12.74	11.87	6.99	5.24	9.30	9.27	11.94	9.67	7.21	5.74	7.39	6.33	6.44
Tb	1.88	1.72	1.02	0.76	1.46	1.43	1.82	1.50	1.05	0.82	1.05	0.98	1.03
Dy	9.40	8.46	5.10	3.77	7.70	7.45	9.43	8.00	5.27	4.17	5.30	5.68	5.98
Ho	1.77	1.54	0.97	0.71	1.52	1.43	1.85	1.52	0.91	0.73	0.93	1.12	1.21
Er	4.91	4.52	2.77	2.00	4.59	4.25	5.59	4.49	2.50	2.00	2.46	3.51	3.73
Yb	4.26	3.86	2.50	1.98	4.64	3.92	6.27	4.29	2.04	1.65	1.97	3.85	3.97
Lu	0.62	0.56	0.38	0.34	0.67	0.57	0.94	0.62	0.30	0.24	0.28	0.59	0.61
Hf	22.01	16.82	11.30	13.18	28.44	28.74	27.78	21.89	5.12	5.25	4.53	21.51	21.85
Ta	9.49	5.77	3.65	3.58	12.99	13.05	13.73	12.63	5.45	4.32	5.21	5.65	6.29
Pb	30.02	53.58	22.93	14.14	127.22	174.66	29.19	44.20	23.65	20.86	17.92	36.01	26.04
Th	40.38	44.33	31.14	11.30	38.06	38.43	43.88	45.46	10.24	11.18	8.02	46.47	47.76
U	8.78	7.58	5.25	3.20	7.72	13.18	4.33	8.71	2.68	2.61	2.27	13.19	10.42
LREE	648.70	703.52	443.05	293.08	489.86	519.22	551.53	518.77	254.12	209.83	259.86	556.04	546.20
HREE	35.58	32.52	19.72	14.80	29.88	28.33	37.83	30.08	19.27	15.35	19.38	22.06	22.97
ΣREE	684.28	736.04	462.77	307.88	519.74	547.55	589.36	548.86	273.39	225.18	279.24	578.10	569.17
δEu	0.96	0.94	0.94	0.94	0.93	0.93	0.95	0.95	0.97	1.00	1.03	1.07	1.13
$(La/Yb)_N$	30.61	38.81	39.81	31.16	20.92	27.05	17.90	25.29	19.85	21.71	19.99	34.02	31.81

LOI: loss on ignition.

Table 3
Sr-Nd isotopic data for the Wajilitag diorite and syenitic rock.

Sample	Rb (ppm)	Sr (ppm)	$^{87}Rb/^{86}Sr$	$^{87}Sr/^{86}Sr$	2σ	$(^{87}Sr/^{86}Sr)_i$	Sm (ppm)	Nd (ppm)	$^{147}Sm/^{144}Nd$	$^{143}Nd/^{144}Nd$	2σ	$(^{143}Nd/^{144}Nd)_i$	$\varepsilon_{Nd(t)}$	T_{DM}^{Nd} (Ma)
Syenite porphyry														
wjl050605-1	83.31	1917.59	0.125712	0.704754	0.000011	0.704198	10.42	66.95	0.094069	0.512615	0.000010	0.512446	3.1	682
wjl050605-2	66.70	1227.72	0.157215	0.704836	0.000013	0.704157	10.88	73.33	0.089690	0.512631	0.000010	0.512470	3.6	639
wjl050605-3	55.49	905.95	0.177254	0.704983	0.000010	0.704226	12.80	76.91	0.100620	0.512648	0.000011	0.512468	3.6	677
wjl050605-4	78.24	1166.63	0.194064	0.704953	0.000012	0.704130	10.91	71.88	0.091736	0.512597	0.000011	0.512432	2.9	692
Diorite														
wjl050710	40.68	700.79	0.167989	0.705187	0.000010	0.704466	8.33	46.26	0.108913	0.512517	0.000010	0.512322	0.7	921
wjl050711	64.23	556.59	0.333906	0.706000	0.000012	0.704632	6.51	37.44	0.105055	0.512478	0.000009	0.512290	0.1	943
wjl050712	26.24	940.16	0.080774	0.704615	0.000042	0.704300	8.56	47.70	0.108529	0.512520	0.000011	0.512325	0.8	913
Aegirine–nepheline syenite														
wjl070201	90.59	2854.85	0.091817	0.704021	0.000014	0.703642	14.86	95.76	0.093848	0.512652	0.000011	0.512474	4.1	634
wjl070202	96.87	2725.81	0.102839	0.704120	0.000196	0.709018	13.96	97.94	0.086174	0.512639	0.000010	0.512475	4.1	611
wjl070203	129.78	1954.68	0.192122	0.704368	0.000025	0.703433	8.08	57.12	0.085476	0.512606	0.000012	0.512444	3.5	647
wjl070204	140.97	1698.18	0.240207	0.704596	0.000012	0.703605	5.91	40.01	0.089259	0.512634	0.000011	0.512465	3.9	633

$(^{147}Sm/^{144}Nd)_{CHUR} = 0.1967$ (Jacobsen and Wasserburg, 1980); $(^{143}Nd/^{144}Nd)_{CHUR} = 0.512638$ (Goldstein et al., 1984); Nd depleted mantle model ages (T_{DM}^{Nd}) were calculated after the formula in Goldstein et al. (1984) using $(^{147}Sm/^{144}Nd)_{DM} = 0.2137$ and $(^{143}Nd/^{144}Nd)_{DM} = 0.51315$ (Peucat et al., 1989) at the present day. $\lambda_{Rb} = 1.42 \times 10^{-11}$ a^{-1} (Steiger and Jager, 1977); $\lambda_{Sm} = 6.54 \times 10^{-12}$ a^{-1} (Lugmair and Marti, 1978).

(Fig. 4), the 6 analytic spots were concordant within error, and yielded a weighted mean $^{206}Pb/^{238}U$ age of 281.4 ± 1.7 Ma (2σ, MSWD = 2.1).

The Hf isotopic results of zircons in the diorite are listed in Supplementary Table 3. The initial ratios of $^{176}Hf/^{177}Hf$ are between 0.282588 and 0.282737 (with an average of 0.282669), and the calculated $\varepsilon Hf(t)$ values range from −0.9 to 4.4 (with an average of 2.0). The Hf depleted mantle model ages (T_{DM}^{Hf}) of diorite range between 733 and 927 Ma.

5.2. Mineral chemistry

A diorite sample (WJL070403) was selected for EPMA analyses (Fig. 5 and Supplementary Tables 4 and 5). The compositions of zoned plagioclase in the diorite range from $An_{40}Ab_{57}Or_3$ in the core to $An_{35}Ab_{63}Or_2$ in the rim, in other words showing 'normal" zonation with decreasing anorthite content from core to rim. Biotite from the samples has high fluorine content (1.6–1.9 wt.%), X_{Mg} values ($Mg/[Mg + Fe^{2+}]$) of 0.73–0.76 and TiO_2 content of 5.0–5.8 wt.%, and low chlorine content (0.13–0.22 wt.%).

5.3. Whole-rock geochemistry

The Wajilitag diorite and syenitic rocks fall in the diorite to nepheline syenite region on the TAS diagram with SiO_2 contents of 52.0–57.3 wt.% (Fig. 6a). The aegirine–nepheline syenites and syenite porphyry plot in the peralkaline to weakly peraluminous fields (Fig. 6b). On Harker diagrams (Fig. 7), Fe_2O_{3t}, TiO_2, MgO and P_2O_5 are negatively correlated with SiO_2 content, suggesting the dominant role of fractional crystallization during the formation of these rocks. The decreasing trends of TiO_2 and P_2O_5 illustrate fractionation of ilmenite and apatite.

Table 4
Pb isotopic data for the Wajilitag diorite and syenitic rock.

Samples	$^{206}Pb/^{204}Pb$	2σ	$^{207}Pb/^{204}Pb$	2σ	$^{208}Pb/^{204}Pb$	2σ
Syenite porphyry						
wjl050605-1	18.6644	0.0001	15.5801	0.0001	38.8240	0.0001
wjl050605-4	18.9332	0.0001	15.5583	0.0001	39.3626	0.0001
Diorite						
wjl050710	18.0421	0.0001	15.4563	0.0001	38.0109	0.0001
wjl050711	18.1373	0.0001	15.4577	0.0001	38.2059	0.0001
wjl050712	18.0341	0.0001	15.4130	0.0001	37.9825	0.0001
Aegirine–nepheline syenite						
wjl070201	19.5073	0.0001	15.5957	0.0001	39.8493	0.0001
wjl070203	19.2899	0.0001	15.5878	0.0001	39.8507	0.0001

The alkali mafic rock, syenite porphyry and aegirine-nepheline syenite are rich in total alkalis (11.5–14.3 wt.%), Al_2O_3 (19.4–21.1 wt.%), Zr, Hf and Ba, and have higher Na_2O/K_2O ratios (>1) and lower Mg# (15–35), and K, P and Ti contents. They have higher total rare earth element (REE) abundances (ranging from 308 to 736 ppm) than the diorite. The rocks also have high LREE/HREE (chondrite normalized) ratios (13.2–22.5) than the diorite (Fig. 8a). The alkali mafic rocks and aegirine–nepheline syenite have negative Ta anomalies implying the rutile crystallization, in contrast to the absence of a Ta anomaly for the diorite and syenite porphyry. The significant negative anomalies of K, P and Ti in the alkali mafic rocks and syenitic rocks may be the result of alkali feldspar, apatite and titanite crystallization. The whole-rock geochemical characteristics of diorite samples are generally similar to the syenitic rocks, but some minor differences can be observed. For example, the diorite samples have higher contents of SiO_2, MgO, P_2O_5, CaO, Fe_2O_3, TiO_2, but not Al_2O_3 (Fig. 7). The diorites have higher Mg# values (59–64) and lower alkali contents (8.3–9.7 wt.%) and total REE abundances. The diorite rocks show chondrite-normalized REE patterns that are consistently left-sloping, but the LREE/HREE ratios of the diorite rocks are consistently lower than for syenitic rocks (Fig. 8a). On trace element spider diagrams (Fig. 8b), the diorite samples do not show strongly enrichment or loss in LILE and HFSE. All rock samples lack Eu anomalies in Fig. 8a.

5.4. Whole-rock Sr–Nd–Pb isotopic compositions

The initial isotope ratios were calculated at t = 275 Ma. The samples of syenite porphyry and aegirine–nepheline syenite have variable Sm and Nd contents but relatively constant $^{147}Sm/^{144}Nd$ and $^{143}Nd/^{144}Nd$ ratios ranging from 0.0855 to 0.1006 and 0.51243 to 0.51248, respectively, corresponding to $\varepsilon Nd(t)$ values of 2.9–4.1. The diorite samples have different $^{147}Sm/^{144}Nd$ and $^{143}Nd/^{144}Nd$ ratios ranging from 0.1051 to 0.1089 and from 0.51229 to 0.51233, respectively, corresponding to $\varepsilon Nd(t)$ values of 0.09–0.78. The Nd depleted mantle model ages (T_{DM}^{Nd}) of syenitic rocks range from 611 to 692 Ma whereas the T_{DM}^{Nd} of diorite samples are 913–943 Ma.

Among eleven samples analyzed, the diorites and syenitic rocks have lower $^{87}Rb/^{86}Sr$ ratios of 0.0808–0.3339, corresponding to the lower $(^{87}Sr/^{86}Sr)_i$ ratios of 0.70343–0.70583.

Pb isotopic ratios are also distinctive, with the $^{206}Pb/^{204}Pb$ ratios of the syenite, aegirine–nepheline syenite and diorite samples ranging from about 18.66 to 18.93, 19.29 to 19.51 and 18.03 to 18.14, respectively (Table 4).

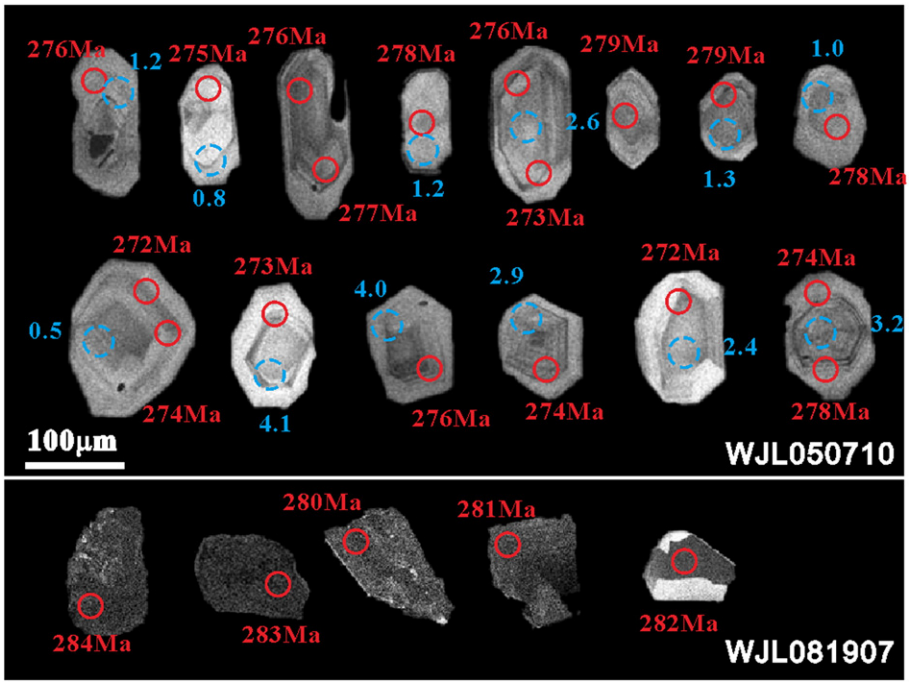

Fig. 3. CL (cathodeluminescence) images of dated zircon crystals from the diorite (WJL050710) and alkali mafic rock (WJL081907) in the Wajilitag area.
Note: The red circles, blue circles and numbers represent the analyzed spots for zircon U–Pb dating, Hf isotopes and $\varepsilon Hf(t)$, respectively.

6. Discussion

6.1. The timing of emplacement of the Wajilitag complex and its vanadium titano-magnetite mineralization

A U–Pb age of ca. 275 Ma for the youngest units of the complex and an age of ca. 281 Ma for the large-scale Fe–Ti oxides mineralized were determined in this study. Based on the field observation, the alkali mafic dikes intruded into the clinopyroxenite, and the latter contained the large Fe–Ti oxide deposit. The zircon U–Pb dating of alkali mafic dike yielded the age of 281.4 ± 1.7 Ma, which confirms that the clinopyroxenite unit and its associated Fe–Ti oxide deposit formed earlier than ca. 281 Ma. Furthermore, the diorite body was located on the top of the complex, and the age of 275.2 ± 1.2 Ma obtained from the diorite may imply for the terminal age of the complex.

In the Tarim LIP, igneous activity occurred from ca. 300 Ma to 270 Ma (Table 1) (Li, 2013; Li et al., 2011; Xu et al., 2014; D.Y. Zhang et al., 2013). It is noted that the basalts are regarded as one of the earliest units of the Tarim LIP (Z.L. Li et al., 2012; Tian et al., 2010; X. Yu et al., 2011; Zhang et al., 2012) and the mafic–ultramafic layered intrusions, intermediate-felsic bodies, mafic dikes and bimodal dikes make up the younger part of the Tarim LIP (Li et al., 2011; Yang et al., 2007; Zhang et al., 2008). From Table 1, it is apparent that the dikes of the Tarim LIP, were emplaced over an age range of ca. 284–272 Ma. The age of the alkali mafic dike is 281 Ma and provides a constraint on the timing of emplacement of the clinopyroxenite and associated Fe–Ti oxide mineralization.

It is noted that the emplacement age of the diorite is identical with a zircon SHRIMP U–Pb age of 272 ± 1.2 Ma for a quartz syenite dike of Xiaohaizi area in the Bachu County (Yang et al., 2007) and is similar to

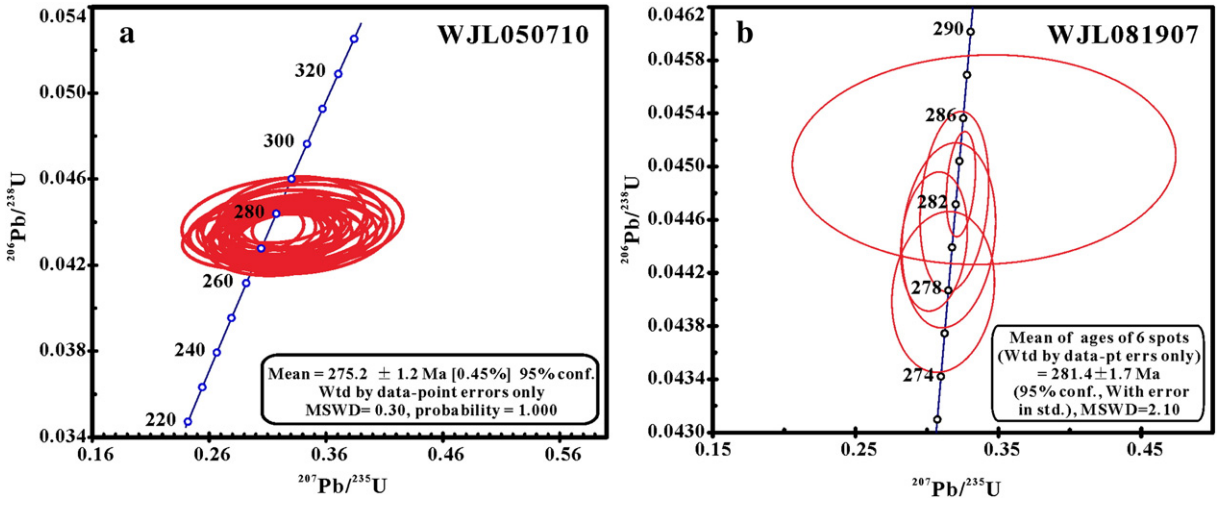

Fig. 4. (a) LA–MC–ICPMS U–Pb zircon concordia diagrams for the diorite (WJL050710) and (b) SHRIMP U–Pb zircon concordia diagram for alkali mafic dike (WJL081907) belonging to the Wajilitag intrusive complex.

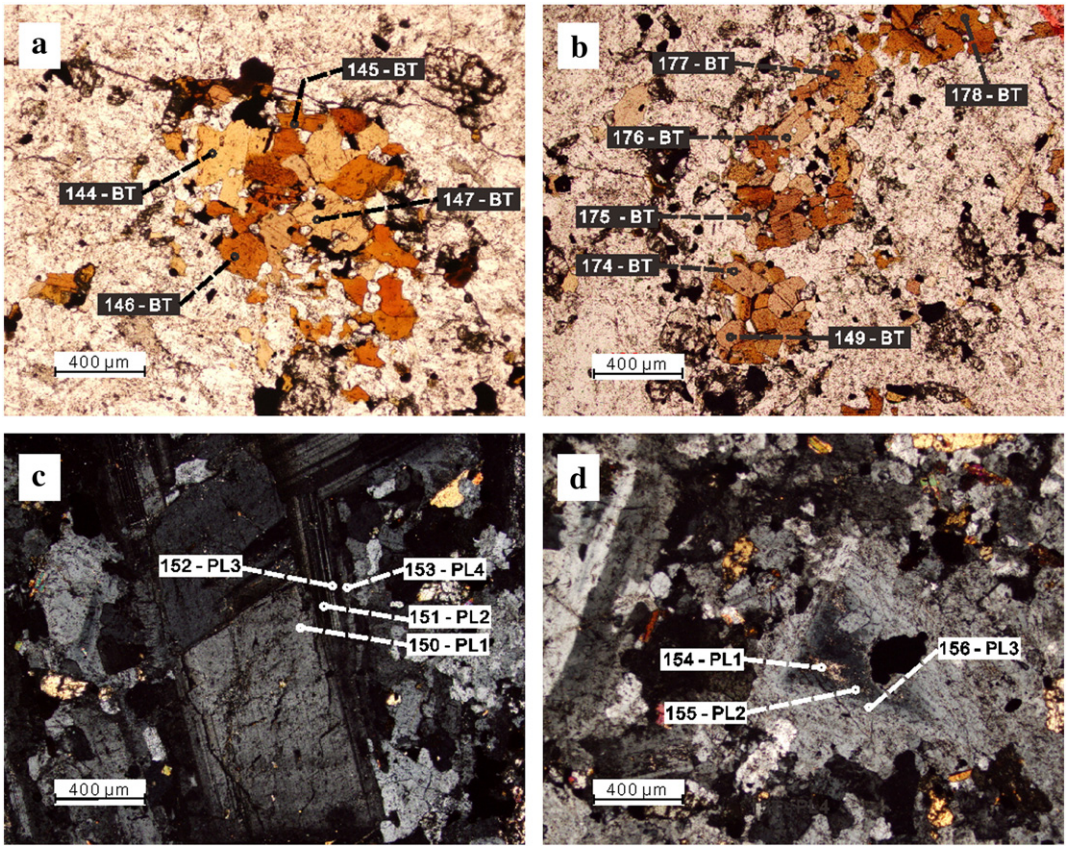

Fig. 5. (a) and (b), and (c) and (d) showing analyzed point locations of biotites and plagioclases from the diorite, respectively.

the zircon U–Pb age of 274 ± 2 Ma for a quartz syenite in the Wajilitag intrusive complex (Zhang et al., 2008). Combined with other published U–Pb data, it can be deduced that ca. 275 Ma of the emplacement time of the Wajilitag intrusive complex matches the ages for bimodal dikes in Bachu County and possibly represents the terminal age of Wajilitag complex formation.

Based on the ages we obtained for the alkali mafic rock and diorite, it can be speculated that the duration of the Wajilitag intrusive complex magmatism is from at least 281 Ma to 275 Ma. In addition, the alkali mafic dikes were emplaced earlier than the diorite and syenitic rocks in the Wajilitag complex, and there are diverse periods of mafic dike emplacement in Bachu area.

6.2. Origin of the syenitic rocks and diorites

The negative correlations of MgO and Fe_2O_{3T} vs. SiO_2 contents of the Tarim Permian intrusions most likely indicate fractional crystallization from a magma source. In Harker diagrams (Fig. 7), all Bachu intrusive rock samples show a clear trend, which reflects a strong fractional crystallization process. It is obvious that the intrusive rocks from ultramafic

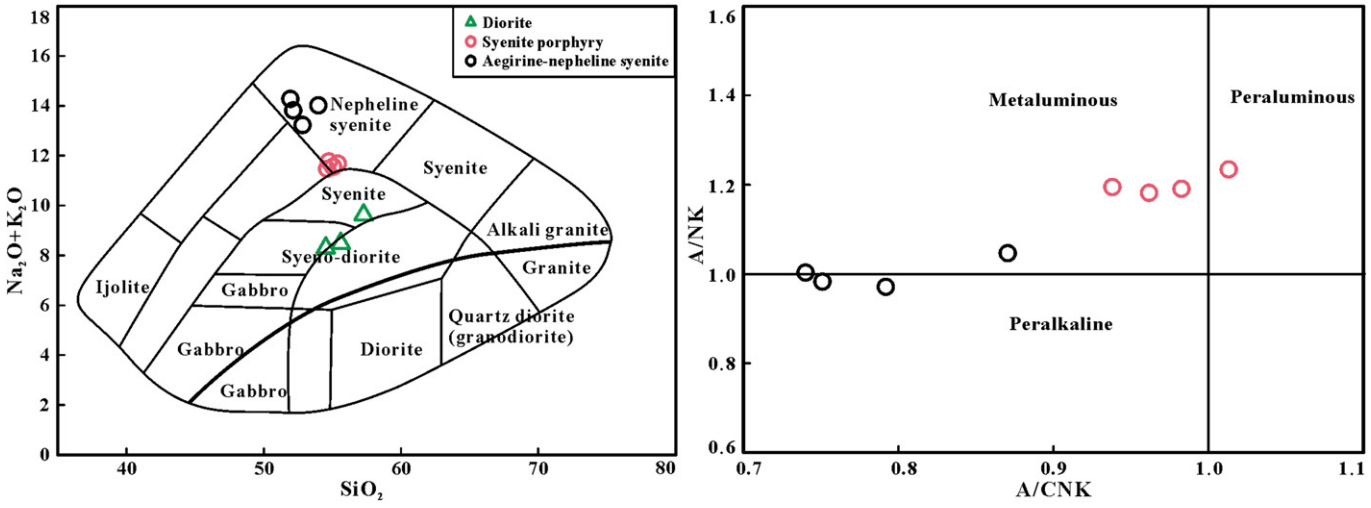

Fig. 6. (a) SiO_2 versus $K_2O + Na_2O$ classification diagram (Cox et al., 1979); (b) A/NK versus A/CNK plot showing the weakly peralkaline to weakly peraluminous character of Wajilitag syenitic rocks (Maniar and Piccoli, 1989). A = Al_2O_3, N = Na_2O, K = K_2O and C = CaO.

to felsic in composition show significant fractional crystallization with a weak contribution from crustal assimilation (Fig. 9). The alkali mafic rocks and syenitic rocks are rich in alkalis, and the alkalis in the diorite are relatively high, inferring that they formed in a within-plate environment. The alkali mafic rocks and syenitic rocks show enrichment of HFSE (e.g., Th, Nb, Zr and Hf) and depletion of K, P and Ti, implying fractional crystallization of alkali feldspar, apatite and ilmenite. In addition, trace element and REE patterns for the diorite are similar to the syenitic rocks, with both exhibiting no significant enrichment or loss of HFSE or LILE.

Biotite provides an important host for halogens. In natural biotites, the OH group may be completely replaced by fluorine, so the F/(F + Cl + OH) value can be nearly 1 and the amount of chlorine substitution can be as low as Cl/(F + Cl + OH) of <0.1 (Munoz, 1984). Magnesium and ferrous contents in biotite are directly related to F–Cl–OH exchange between biotite and hydrothermal fluids (Munoz, 1984). F/(F + Cl + OH) values (0.19–0.22) and high IV(F) and IV(F/Cl) values (Supplementary Table 3) from diorite samples indicate low water fugacity conditions. Therefore, the high temperature stability of biotite determined in water undersaturated conditions (Munoz, 1984) may not apply in this case. The samples have high fluorine contents (1.6–1.9 wt.%) with constant amounts of TiO_2 (5.0–5.8 wt.%) in biotite, which are consistent with relatively high temperature conditions inferred for biotite. Combined with the high TiO_2 and halogen content in biotite, we can speculate the environment for biotite formation may be under high temperature and low water fugacity conditions and a relatively deep depth in the crust.

The Wajilitag rocks that we have studied have low $(^{87}Sr/^{86}Sr)_i$ ratios ranging between 0.70343 and 0.70583 and positive $\varepsilon Nd(t)$ values of 0.09–4.12. These samples fall in near the FOZO area (Hart et al., 1992; Stracke et al., 2005) in the $(^{87}Sr/^{86}Sr)_i$ vs. $\varepsilon Nd(t)$ diagram (Fig. 10), suggesting they may be derived from a plume or the degassed mantle. Among the diorite and syenitic rocks, there is a weak evolutionary trend from aegirine–nepheline syenite to diorite, which is probably due to fractional crystallization. Moreover, the $\varepsilon Hf(t)$ values in zircon of basalts and intrusive rocks in Tarim LIP (Fig. 11) also show an evolutionary trend from an enriched mantle to depleted mantle source components. On the Pb isotopic graph (Fig. 12), there is a trend from basalts and mafic–ultramafic rocks in enriched mantle source to syenitic rocks and diorite on the DMM-FOZO array. There is a tendency for the basalts from the Tarim LIP to be derived from an enriched mantle component

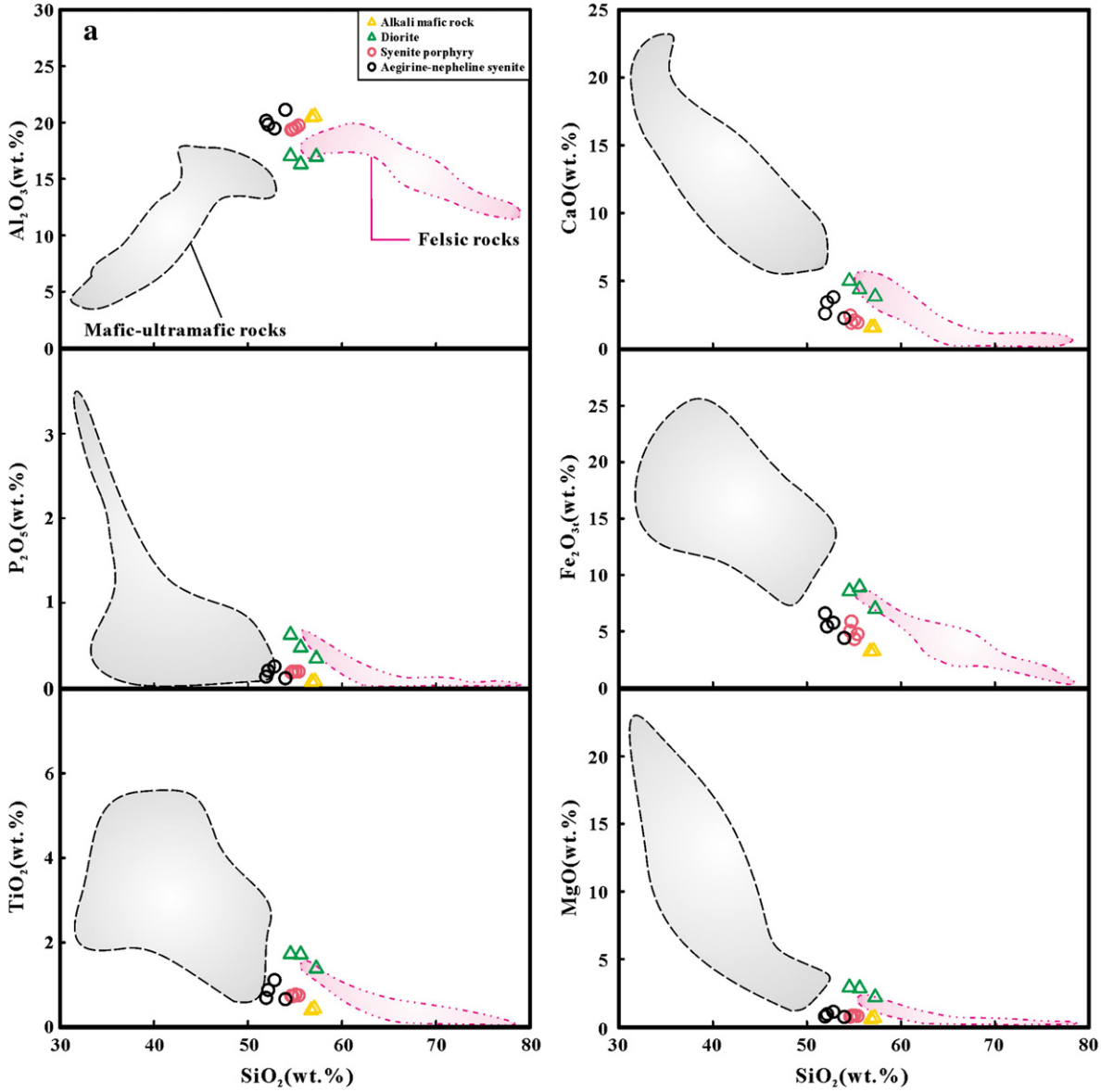

Fig. 7. (a) SiO_2 versus major elements and (b) SiO_2 versus trace element diagrams for the Tarim LIP rocks. Note: The data of mafic–ultramafic and felsic rocks are from C.L. Zhang et al. (2010), Sun et al. (2008), Y.Q. Li et al. (2010), Yang et al. (2007), and Zhang et al. (2008).

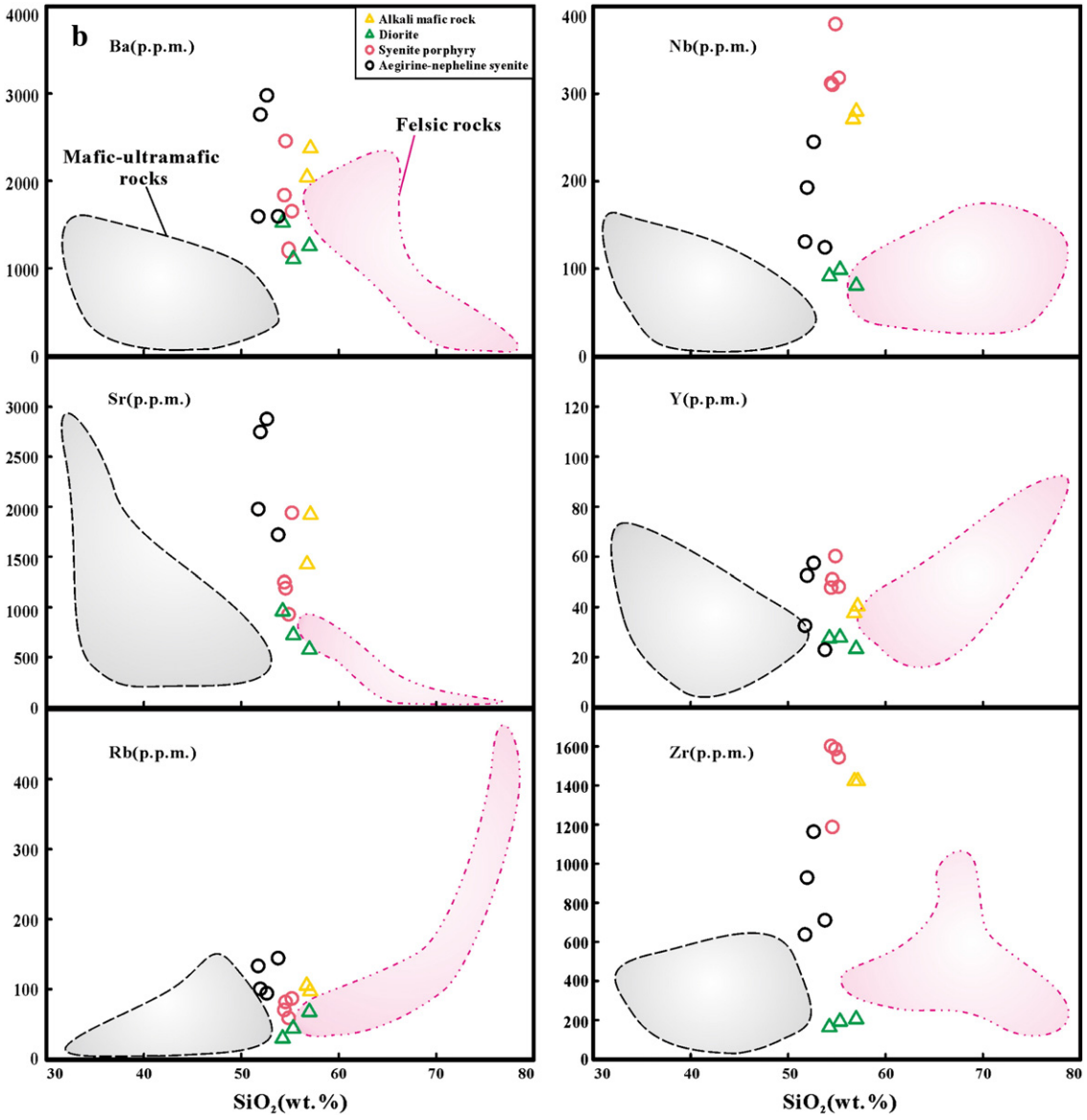

Fig. 7 (*continued*).

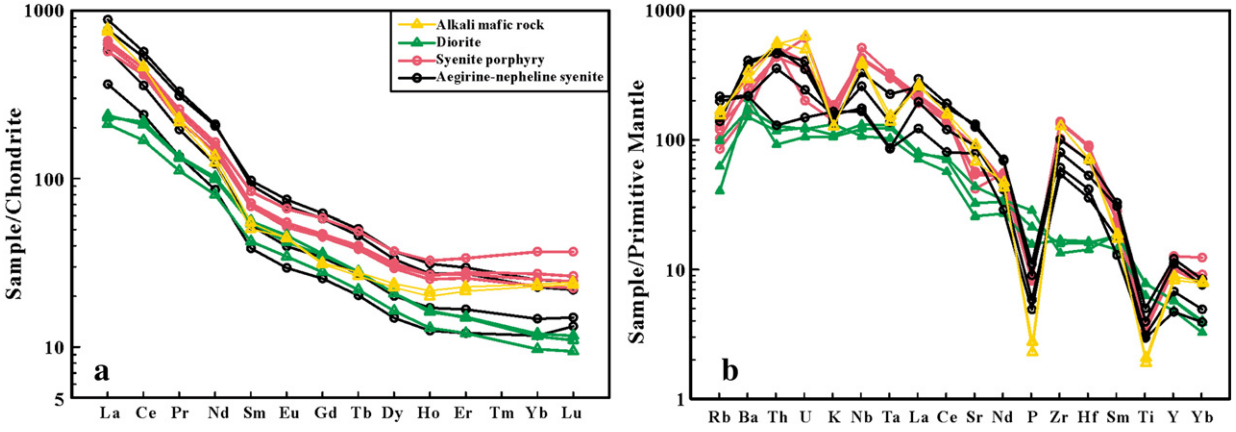

Fig. 8. (a) Chondrite normalized REE patterns, and (b) primitive mantle normalized spidergrams for the intermediate igneous rocks. The normalization values of primitive mantle and chondrite are from Sun and McDonough (1989).

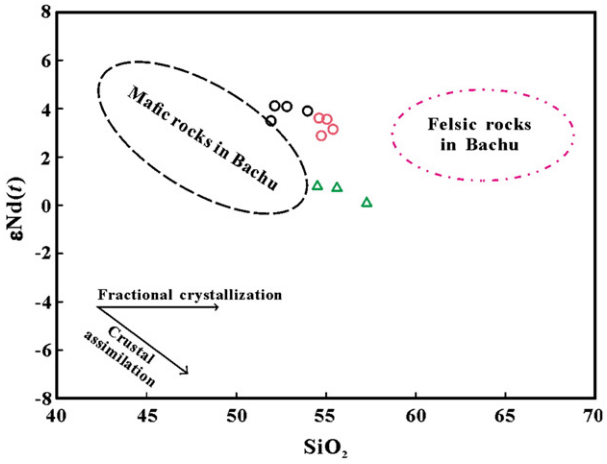

Fig. 9. εNd(t) versus SiO_2 for the Wajilitag complex rocks.
Note: The fields for mafic rocks and felsic rocks are from C.L. Zhang et al. (2010), Sun et al. (2008), Yang et al. (2007), Yu (2009), Zhang et al. (2008), and Zhou et al. (2009). Symbols are the same as in Fig. 7.

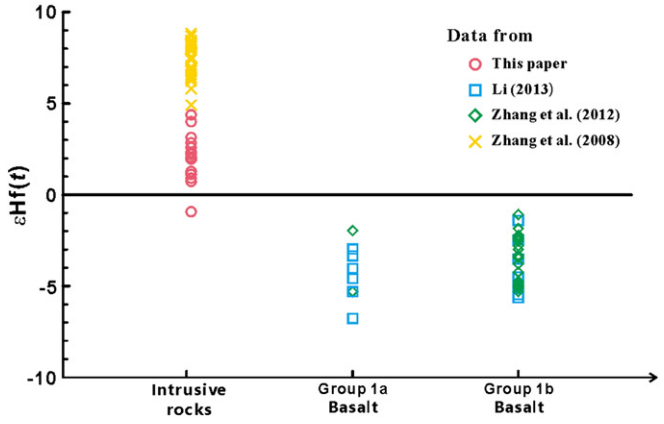

Fig. 11. The zircon εHf(t) values of the Group 1a basalt, Group 1b basalt and intrusive rocks in the Tarim LIP.
Note: the other data are from Zhang et al. (2008), D.Y. Zhang et al. (2010), Zhang et al. (2012), and Li (2013).

whereas the Tarim intrusive rocks are from a FOZO-like mantle component (Fig. 13). We suggest that the Wajilitag complex may be mainly derived from plume mantle (FOZO-type), but may also have minor addition of an EMII-type OIB component which had some lithospheric mantle interacted beneath the Tarim Basin.

Combined with the previous studies of coeval basalts and intrusive rocks, this study of the geochemistry, Sr–Nd–Pb isotopes and zircon Hf isotopes of the Wajilitag syenitic rocks and diorite confirms that the Wajilitag intrusive rocks are derived mainly from a relatively depleted plume mantle source (FOZO-type) which assimilated recycled old enriched lithospheric mantle, and then underwent strong fractional crystallization within the crust.

6.3. Implication for the Tarim LIP evolution history

Diorite and syenitic rocks associated with LIPs are typically emplaced during the later part of the LIP event (De Waal and Armstrong, 2000; Shellnutt et al., 2011; Song et al., 2008; Zhong et al., 2011). In the Emeishan LIP, most syenites and A-type granites were derived by differentiation of basaltic magmas (Shellnutt and Jahn, 2010; Shellnutt and Zhou, 2007; Shellnutt et al., 2009a,b, 2012; Zhong et al., 2007, 2009, 2011) or by mixing between crustal melts and primary basaltic magmas (Xu et al., 2008). On the εNd(t) vs. $(^{87}Sr/^{86}Sr)_i$ isotope plot (Fig. 10), the rocks in this paper fall in near the FOZO area, showing the similar characteristics to the other Bachu Permian mafic–ultramafic rocks (Yang

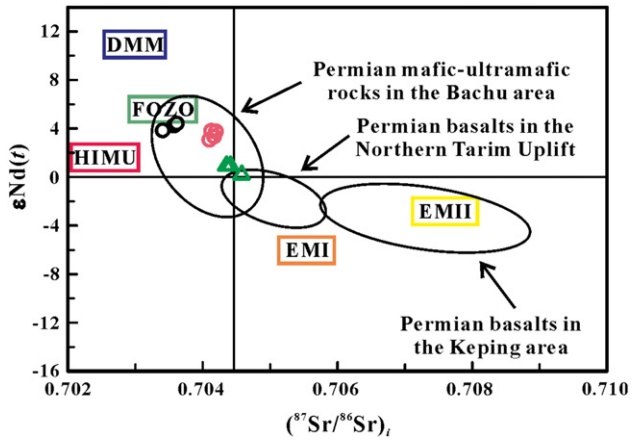

Fig. 10. εNd(t) vs. initial $^{87}Sr/^{86}Sr$ diagram for Wajilitag syenitic rocks and diorites.
The fields of DMM, FOZO, EMI, EMII and HIMU are from Hart (1984), Hofmann (2003) and Zindler and Hart (1986). The other data are from C.L. Zhang et al. (2010), X. Yu et al. (2011), Zhang et al. (2008), and Zhou et al. (2009). Symbols are the same as in Fig. 7.

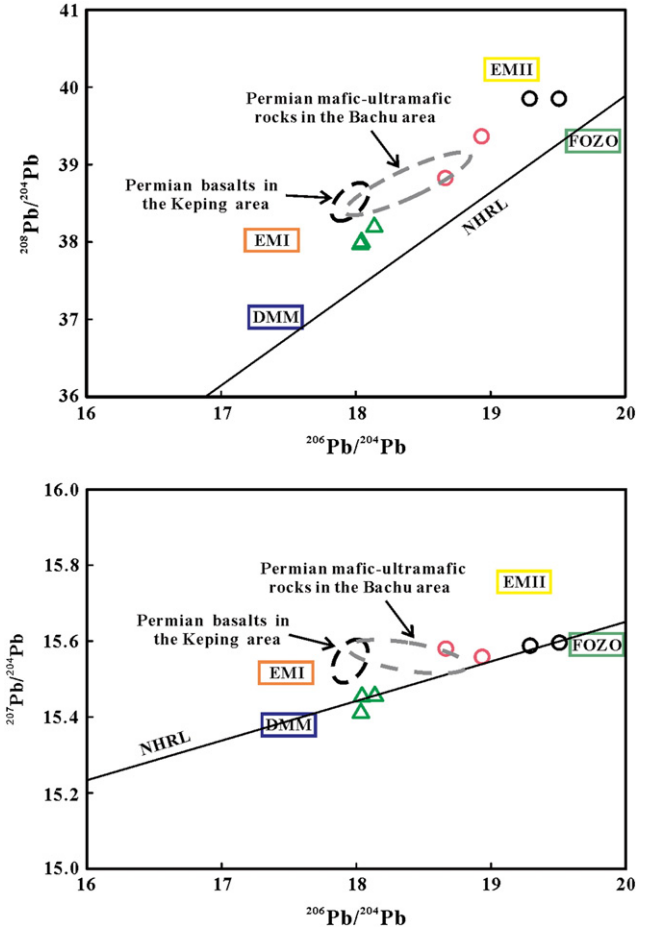

Fig. 12. $^{206}Pb/^{204}Pb$ versus $^{208}Pb/^{204}Pb$ and $^{206}Pb/^{204}Pb$ versus $^{207}Pb/^{204}Pb$ plots for the Wajilitag syenitic rocks and diorites.
The fields of DMM, FOZO, EMI and EMII and Northern Hemisphere Reference Line (NHRL) are from Zindler and Hart (1986), Hart (1984), Hofmann (2003) and Stracke et al. (2005). The other plotted data are from Zhou et al. (2009). Symbols are the same as in Fig. 7.

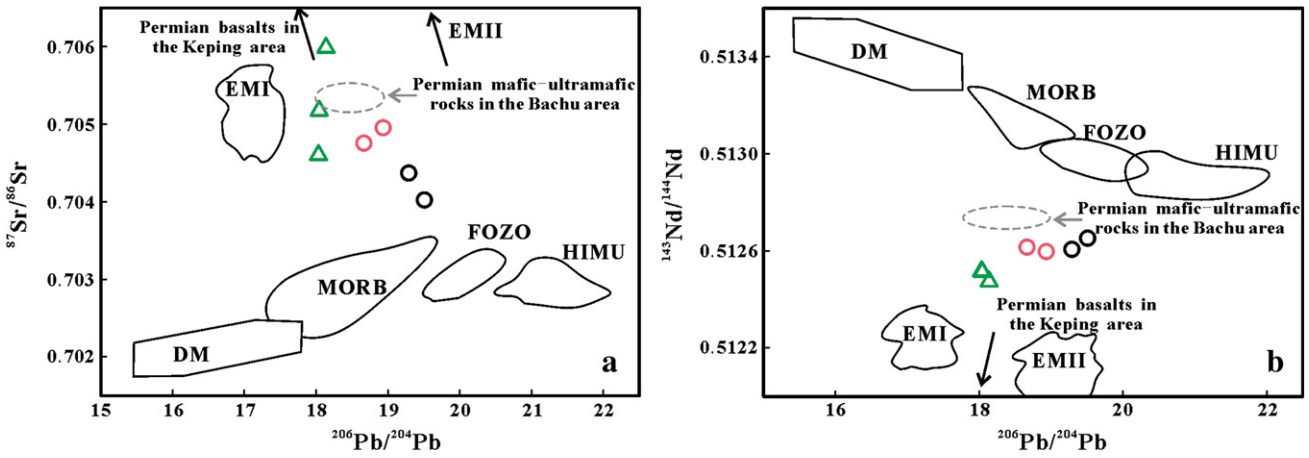

Fig. 13. (a) $^{206}Pb/^{204}Pb$ versus $^{87}Sr/^{86}Sr$ and (b) $^{206}Pb/^{204}Pb$ versus $^{143}Nd/^{144}Nd$ plots for the Wajilitag syenitic rocks and diorites. The data sources are the same as in Fig. 12. Symbols are the same as in Fig. 7.

et al., 2007; Zhang et al., 2008). It's obvious that the Tarim LIP rocks have a significant trend followed a temporal evolution from the basalt to intrusive rocks. The Keping basalts have the highest $(^{87}Sr/^{86}Sr)_i$ and lowest $\varepsilon Nd(t)$ values indicating an enriched mantle source (dominated by an EMII component). As the later magmatic pulse of the Tarim LIP, the intrusive rocks in Bachu area show higher $\varepsilon Nd(t)$ values than the basalts, implying an injection of the more depleted mantle source components, probably a FOZO type plume mantle source.

On the other hand, zircon Hf isotopic data of Tarim LIP basalts and intrusive rocks (Li, 2013; Zhang et al., 2008, 2012) indicate distinct magma sources (Fig. 11). As seen in Fig. 11, the basalts from Keping area have the lowest negative $\varepsilon Hf(t)$ values, however, the intrusive rocks in the Wajilitag complex almost show the positive $\varepsilon Hf(t)$ values, which implies that the magma sources changed from enriched mantle to relatively depleted mantle through the protracted duration of the Tarim LIP. The Hf isotopes of the diorite are similar to the Hf isotopic results from the quartz syenite in the Wajilitag intrusion (Zhang et al., 2008). Both of them have positive zircon $\varepsilon Hf(t)$ values, but the $\varepsilon Hf(t)$ values from the diorite range from -0.9 to 4.4 with an average of 2.0 which are lower than the $\varepsilon Hf(t)$ values from the quartz syenite (5.5–8.9) in the Wajilitag complex (Zhang et al., 2008) (Fig. 11). The difference of Hf isotopes between diorite and quartz syenite indicates an evolutionary trend from the diorite to quartz syenite.

Moreover, the T_{DM}^{Hf} of diorite range from 927 Ma to 733 Ma and are older than the model ages of 702-546 Ma for the quartz syenites (Zhang et al., 2008) and are younger than the model ages of 1200-960 Ma for the basalts in the Keping area (Li, 2013; D.Y. Zhang et al., 2010; Zhang et al., 2012). Compared to the older Hf model ages of Keping basalts, the rocks in the Wajilitag complex show younger model ages, reflecting that the source of Tarim LIP originated from the EMII-type OIB mantle component to FOZO-like plume mantle.

Based on field occurrence, U–Pb age, petrochemistry and isotope characteristics mentioned above, combined with regional geology and magmatic evolutional history from previous studies (Li, 2013; Li et al., 2011; Z.L. Li et al., 2012; Yang et al., 2007; Zhang et al., 2008, 2012; Zhou et al., 2009), our study suggests that the diorites of the Wajilitag complex may form through crystal fractionation of the mafic magmatism to become the later rock units of the Wajilitag complex and Tarim LIP, and the source of Wajilitag complex probably was FOZO-like plume mantle. In addition, the basalts and mafic–ultramafic intrusions in Tarim LIP, exhibit a regional source of this LIP changes from the enriched mantle (EMII type) to FOZO-like mantle plume source.

7. Conclusion

Based on the U-Pb ages, geochemical data, Sr–Nd–Pb isotopes and zircon Hf isotope analyses of the Wajilitag alkali mafic dikes, diorite and syenitic rocks, we summarized as follows.

(1) The zircon U–Pb ages of the alkali mafic dike and diorite in the Wajilitag complex are 281.4 ± 1.7 Ma and 275.2 ± 1.2 Ma, respectively. It can be deduced that the ages of ca. 275 Ma and ca. 281 Ma indicate the terminal emplacement time of the Wajilitag intrusive complex and Fe–Ti oxides mineralization time, respectively. The former is consistent with previously published age constraints on mafic dikes and bimodal dikes in the Bachu area.

(2) The higher fluorine and TiO_2 contents and low chlorine contents in biotite of the diorite in the Wajilitag complex indicate that the biotite formed under high temperature and low water fugacity conditions and a deep depth in the crust.

(3) The evidence of lower $(^{87}Sr/^{86}Sr)_i$, and positive high $\varepsilon Hf(t)$ and $\varepsilon Nd(t)$ from the Wajilitag complex in this study suggests a depleted source (perhaps FOZO) reflecting a plume mantle source with minor contamination by an enriched component (dominated by EMII). Some evolved rocks (e.g., diorites) also experienced fractional crystallization from initially derived basaltic magma. In addition, geochemistry, Sr-Nd-Pb isotopes and Nd depleted mantle model ages indicate a magmatic evolutionary trend from the diorite to syenitic rocks.

(4) The zircon U–Pb age and geochemistry of the newly discovered alkali mafic dike which intruded into the clinopyroxenite, indicate the formation time of the clinopyroxenite and Fe–Ti oxide mineralization could be earlier than 281 Ma. Compared with the ages for mafic dikes and bimodal dikes in Bachu area, it can be concluded that the dikes formed over a wide time range from 284 to 272 Ma.

(5) Combined with the previous study of Permian different rock types in Tarim Basin, it can be deduced (based on published data) that the Wajilitag intrusive complex is regarded to belong to a younger pulse of the Permian Tarim LIP. Along with Early Permian basalts erupted and then mafic–ultramafic to felsic rocks intruded in Tarim Basin, the Tarim LIP rocks were derived from mantle source which changed from the enriched mantle component (dominated by EMII) mainly for the basalts to a depleted source (similar to FOZO-type mantle plume) for intrusive rocks, followed by strong fractional crystallization in crustal magma chambers to produce the more evolved phases (i.e., diorite and syenites).

Supplementary data to this article can be found online at http://dx.doi.org/10.1016/j.lithos.2014.09.005.

Acknowledgments

The authors express great thanks to C. Yang, H.Q. Xie, R.L. Fan and N. Li of Beijing SHRIMP Center and J.Z. Geng of Tianjin Institute of Geology and Mineral Resources for help and guidance in zircon U–Pb isotopic analyses, C.F. Li and J.H. Guo of IGGCAS for guidance in Sr–Nd–Pb isotope analyses, Y. Liu and L. Zhang of GIGCAS for assistance in major element analyses and Hf isotope measurement and C.H. Langmuir and Z.X. Chen of Harvard University for help in trace element analyses. The authors also appreciate the help from X. Yu of SIOSOA for the fieldwork and J. Zhou, X.Q. Yang and Y.Z. Hu of Zhejiang University for geochemical analyses. This work was supported by the National Basic Research Program of China (2011CB808902 and 2007CB411303), National Natural Science Foundation of China (40930315 and 41072048), Research Funds for the Doctoral Program of Higher Education of China (20110101110001) and State Key Laboratory of Ore Deposit Geochemistry, Institute of Geochemistry, CAS (201208).

References

Belousova, E.A., Griffin, W.L., O'Reilly, S.Y., Fisher, N.I., 2002. Igneous zircon: trace element composition as an indicator of source rock type. Contributions to Mineralogy and Petrology 143 (5), 602–622.

Bézos, A., Escrig, S., Langmuir, C.H., Michael, P.J., Asimow, P.D., 2009. Origins of chemical diversity of back-arc basin basalts: a segment-scale study of the Eastern Lau Spreading Center. Journal of Geophysical Research 114 (B06212), 1–25.

Borisenko, A.S., Sotnikov, V.I., Izokh, A.E., Polyakov, G.V., Obolensky, A.A., 2006. Permo-Triassic mineralization in Asia and its relation to plume magmatism. Russian Geology and Geophysics 47, 166–182.

Cao, J., Wang, C.Y., Xing, C.M., Xu, Y.G., 2014. Origin of the early Permian Wajilitag igneous complex and associated Fe–Ti oxide mineralization in the Tarim large igneous province, NW China. Journal of Asian Earth Sciences 84, 51–68.

Chen, H.L., Yang, S.F., Dong, C.W., Jia, C.Z., Wei, G.Q., Wang, Z.G., 1997a. The discovery of Early Permian basic rock belt in Tarim basin and its tectonic meaning. Geochimica 26 (6), 77–87 (in Chinese with English abstract).

Chen, H.L., Yang, S.F., Dong, C.W., Zhu, G.Q., Jia, C.Z., Wei, G.Q., Wang, Z.G., 1997b. Research on geological thermal event of Tarim basin. Chinese Science Bulletin 42 (10), 1096–1099 (in Chinese).

Chen, M.M., Tian, W., Zhang, Z.L., Pan, W.Q., Song, Y., 2010. Geochronology of the Permian basic-intermediate-acidic magma suite from Tarim, Northwest China and its geological implications. Acta Petrologica Sinica 26 (2), 559–572 (in Chinese with English abstract).

Cox, K.G., Bell, J.D., Pankhurst, R.J., 1979. The interpretation of igneous rocks.

De Waal, S.A., Armstrong, R.A., 2000. The age of the Marble Hall diorite, its relationship to the Uitkomst Complex, and evidence for a new magma type associated with the Bushveld igneous event. South African Journal of Geology 103 (2), 128–140.

Gao, Y.S., 2007. Geological characteristics of Wajilitag vanadic titanomagnetite deposit and its prospecting recommendations. Xinjiang Iron and Steel 102, 8–9 (in Chinese).

Goldstein, S.L., O'Nions, R.K., Hamilton, P.J., 1984. A Sm–Nd isotopic study of atmospheric dusts and particulates from major river systems. Earth and Planetary Science Letters 70, 221–236.

Hart, S.R., 1984. A large-scale isotope anomaly in the southern hemisphere mantle. Nature 309, 753–757.

Hart, S.R., 1988. Heterogeneous mantle domains: signatures, genesis and mixing chronologies. Earth and Planetary Science Letters 90 (3), 273–296.

Hart, S.R., Hauri, E.H., Oschmann, L.A., Whitehead, J.A., 1992. Mantle plumes and entrainment: isotopic evidence. Science 256 (5056), 517–520.

Hofmann, A.W., 2003. Sampling mantle heterogeneity through oceanic basalts: isotopes and trace elements. Treatise on Geochemistry 2, 61–101.

Hou, K.J., Li, Y.H., Tian, Y.R., 2009. In situ U–Pb zircon dating using laser ablation-multi ion counting-ICP-MS. Mineral Deposits 28 (4), 481–492 (in Chinese with English abstract).

Iizuka, Y., Bellwood, P., Hung, H.C., Dizon, E.Z., 2005. A non-destructive mineralogical study of nephritic artifacts from Itbayat Island, Batanes, northern Philippines. Journal of Austronesian Studies 1, 80–105.

Jackson, S.E., Pearson, N.J., Griffin, W.L., Belousova, E.A., 2004. The application of laser ablation-inductively coupled plasma-mass spectrometry to in situ U–Pb zircon geochronology. Chemical Geology 211, 47–69.

Jacobsen, S.B., Wasserburg, G.J., 1980. Sm–Nd isotopic evolution of chondrites. Earth and Planetary Science Letters 50, 139–155.

Jia, C.Z., 1997. Tectonic Characteristics and Oil-Gas, Tarim Basin, China. Petroleum Industry Press, Beijing, pp. 1–438 (in Chinese).

Jia, C.Z., Wei, G.Q., Yao, H.J., 1995. Tectonic Evolution of Tarim and Regional Tectonics. Petroleum Industry Press, Beijing, pp. 1–174 (in Chinese).

Jiang, C.Y., Zhang, P.B., Lu, D.R., Bai, K.Y., Wang, Y.P., Tang, S.H., Wang, J.H., Yang, C., 2004. Petrology, geochemistry and petrogenesis of the Kalpin basalts and their Nd, Sr and Pb isotopic compositions. Geological Review 50 (5), 492–500 (in Chinese with English abstract).

Li, Y.Q., 2013. Study on Magma Dynamics and Ore Potential of the Early Permian Tarim Large Igneous Province. Doctoral Dissertation of Zhejiang University,pp. 1–122, (in Chinese with English abstract).

Li, Y., Su, W., Kong, P., Qian, Y.X., Zhang, K.L., Zhang, M.L., Chen, Y., Cai, X.Y., You, D.H., 2007. Zircon U–Pb ages of the Early Permian magmatic rocks in the Tazhong–Bachu region, Tarim Basin by LA–ICP–MS. Acta Petrologica Sinica 23 (5), 1097–1107 (in Chinese with English abstract).

Li, Z.L., Yang, S.F., Chen, H.L., Langmuir, C.H., Yu, X., Lin, X.B., Li, Y.Q., 2008. Chronology and geochemistry of Taxinan basalts from the Tarim: evidence for Permian plume magmatism. Acta Petrologica Sinica 24 (5), 959–970 (in Chinese with English abstract).

Li, X.H., Long, W.G., Li, Q.L., Liu, Y., Zheng, Y.F., Yang, Y.H., Chamberlain, K.R., Wan, D.F., Guo, C.H., Wang, X.C., Tao, H., 2010. Penglai zircon megacrysts: a potential new working reference material for microbeam determination of Hf–O isotopes and U–Pb age. Geostandards and Geoanalytical Research 34 (2), 117–134.

Li, Y.Q., Li, Z.L., Chen, H.L., Yang, S.F., Yu, X., 2010. PGE and geochemistry of Wajilitag ultramafic cryptoexplosive brecciated rocks from Tarim Basin: implications for petrogenesis. Acta Petrologica Sinica 26 (11), 3307–3318 (in Chinese with English abstract).

Li, Z.L., Chen, H.L., Song, B., Li, Y.Q., Yang, S.F., Yu, X., 2011. Temporal evolution of the Permian large igneous province in Tarim Basin in northwestern China. Journal of Asian Earth Sciences 42 (5), 917–927.

Li, Y.Q., Li, Z.L., Chen, H.L., Yang, S.F., Yu, X., 2012. Mineral characteristics and metallogenesis of the Wajilitag layered mafic–ultramafic intrusion and associated Fe–Ti–V oxide deposit in the Tarim large igneous province, northwest China. Journal of Asian Earth Sciences 49, 161–174.

Li, Z.L., Li, Y.Q., Chen, H.L., Santosh, M., Yang, S.F., Xu, Y.G., Langmuir, C.H., Chen, Z.X., Yu, X., Zou, S.Y., 2012. Hf isotopic characteristics of the Tarim Permian large igneous province rocks of NW China: implication for the magmatic source and evolution. Journal of Asian Earth Sciences 49, 191–202.

Liu, Y.S., Gao, S., Hu, Z.C., Gao, C.G., Zong, K.Q., Wang, D.B., 2009. Continental and oceanic crust recycling-induced melt–peridotite interactions in the Trans-North China Orogen: U–Pb dating, Hf isotopes and trace elements in zircons from mantle xenoliths. Journal of Petrology 51 (1–2), 537–571.

Ludwig, K.R., 2003. User's Manual for Isoplot 3.00: A Geochronological Toolkit for Microsoft Excel. Special Publication 4. Geochronology Center, Berkeley, pp. 1–70.

Lugmair, G.W., Marti, K., 1978. Lunar initial $^{143}Nd/^{144}Nd$: differential evolution of the lunar crust and mantle. Earth and Planetary Science Letters 39, 349–357.

Maniar, P.D., Piccoli, P.M., 1989. Tectonic discrimination of granitoids. Geological Society of America Bulletin 101 (5), 635–643.

Munoz, J.L., 1984. F–OH and Cl–OH exchange in micas with applications to hydrothermal ore deposits. In: Bailey, S.W. (Ed.), Micas. Reviews in Mineralogy 13, pp. 469–494.

Peucat, J.J., Vidal, P., Bernard-Griffiths, J., Condie, K.C., 1989. Sr, Nd and Pb isotopic systematics in the Archaean low- to high-grade transition zone of southern India: syn-accretion vs post-accretion granulites. Journal of Geology 97, 537–550.

Saal, A.E., Hart, S.R., Shimizu, N., Hauri, E.H., Layne, G.D., Eiler, J.M., 2005. Pb isotopic variability in melt inclusions from the EMI–EMII–HIMU mantle end-members and the role of the oceanic lithosphere. Earth and Planetary Science Letters 240 (3), 605–620.

Shellnutt, J.G., Jahn, B.M., 2010. Formation of the Late Permian Panzhihua plutonic-hypabyssal-volcanic igneous complex: implication for the genesis of Fe–Ti oxide deposits and A-type granites of SW China. Earth and Planetary Science Letters 289, 509–519.

Shellnutt, J.G., Zhou, M.F., 2007. Permian peralkaline, peraluminous and metaluminous A-type granites in the Panxi district, SW China: their relationship to the Emeishan mantle plume. Chemical Geology 243, 286–313.

Shellnutt, J.G., Zhou, M.F., Zellmer, G., 2009a. The role of Fe–Ti oxide crystallization in the formation of A-type granitoids with implications for the Daly gap: an example from the Permian Baima igneous complex, SW China. Chemical Geology 259, 204–217.

Shellnutt, J.G., Wang, C.Y., Zhou, M.F., Yang, Y.H., 2009b. Zircon Lu–Hf isotopic compositions of metaluminous and peralkaline A-type granitic plutons of the Emeishan large igneous province (SW China): constraints on the mantle source. Journal of Asian Earth Sciences 35, 45–55.

Shellnutt, J.G., Jahn, B.M., Zhou, M.F., 2011. Crustally-derived granites in the Panzhihua region, SW China: Implications for felsic magmatism in the Emeishan large igneous province. Lithos 123 (1), 145–157.

Shellnutt, J.G., Denyszyn, S.W., Mundil, R., 2012. Precise age determination of mafic and felsic intrusive rocks from the Permian Emeishan large igneous province (SW China). Gondwana Research 22 (1), 118–126.

Song, B., Zhang, Y.H., Wan, Y.S., Jian, P., 2002. Mount making and procedure of the SHRIMP dating. Geological Review 48, 26–30 (Supp., in Chinese with English abstract).

Song, X.Y., Zhou, M.F., Tao, Y., Xiao, J.F., 2008. Controls on the metal compositions of magmatic sulfide deposits in the Emeishan large igneous province, SW China. Chemical Geology 253 (1), 38–49.

Steiger, R.H., Jager, E., 1977. Subcommission on geochronology: convention on the use of decay constants in geo- and cosmo-chronology. Earth and Planetary Science Letters 36, 359–362.

Stracke, A., Hofmann, A.W., Hart, S.R., 2005. FOZO, HIMU, and the rest of the mantle zoo. Geochemistry, Geophysics, Geosystems 6 (5).

Sun, S.S., McDonough, W.F., 1989. Chemical and isotopic systematics of oceanic basalts: implications for mantle composition and processes. In: Saunders, A.D., Norry, M.J. (Eds.), Magmatism in the Ocean Basalts. Geological Society Special Publication 42, pp. 313–345.

Sun, L.H., Wang, Y.J., Fan, W.M., Zi, J.W., 2008. A further discussion of the petrogenesis and tectonic implication of the mazhashan syenites in the Bachu area. Journal of Jilin University (Earth Science Edition) 38 (1), 8–20 (in Chinese with English abstract).
Tackley, P.J., 2007. Mantle geochemical geodynamics. Treatise on Geophysics 7, 437–505.
Tian, W., Campbell, I.H., Allen, C.M., Guan, P., Pan, W.Q., Chen, M.M., Yu, H.J., Zhu, W.P., 2010. The Tarim picrate–basalt–rhyolite suite, a Permian flood basalt from northwest China with contrasting rhyolites produced by fractional crystallization and anatexis. Contributions to Mineralogy and Petrology 160 (3), 407–425.
Wei, X., Xu, Y.G., 2011. Petrogenesis of Xiaohaizi syenite complex from Bachu area, Tarim. Acta Petrologica Sinica 27 (10), 2984–3004 (in Chinese with English abstract).
Wei, G.J., Liu, Y., Tu, X.L., Liang, X.R., Li, X.H., 2004. Separation of Sr, Sm and Nd in mineral and rock samples using selective specific resins. Rock and Mineral Analysis 23 (1), 11–14 (in Chinese with English abstract).
Wei, X., Xu, Y.G., Feng, Y.X., Zhao, J.X., 2014. Plume-lithosphere interaction in the generation of the Tarim large igneous province, NW China: geochronological and geochemical constraints. American Journal of Science 314 (1), 314–356.
Willbold, M., Stracke, A., 2010. Formation of enriched mantle components by recycling of upper and lower continental crust. Chemical Geology 276 (3), 188–197.
Williams, I.S., 1998. U–Th–Pb geochronology by ion microprobe. Reviews in Economic Geology 7 (1), 1–35.
Wu, F.Y., Yang, Y.H., Xie, L.W., Yang, J.H., Xu, P., 2006. Hf isotopic compositions of the standard zircons and baddeleyites used in U–Pb geochronology. Chemical Geology 234 (1–2), 105–126.
Xu, Y.G., Luo, Z.Y., Huang, X.L., He, B., Xiao, L., Xie, L.W., Shi, Y.R., 2008. Zircon U–Pb and Hf isotope constraints on crustal melting associated with the Emeishan mantle plume. Geochimica et Cosmochimica Acta 72 (13), 3084–3104.
Xu, Y.G., Wei, X., Luo, Z.Y., Liu, H.Q., Cao, J., 2014. The Early Permian Tarim Large Igneous Province: main characteristics and a plume incubation model. Lithos 204, 20–35.
Yang, S.F., Chen, H.L., Dong, C.W., Jia, C.Z., Wang, Z.G., 1996. The discovery of Permian syenite inside Tarim Basin and its geodynamic significance. Geochimica 25 (2), 121–128 (in Chinese with English abstract).
Yang, S.F., Li, Z.L., Chen, H.L., Xiao, W.J., Yu, X., Lin, X.B., Shi, X.G., 2006. Discovery of a Permian quartz syenitic porphyritic dyke from the Tarim Basin and its tectonic implications. Acta Petrologica Sinica 22 (5), 1405–1412 (in Chinese with English abstract).
Yang, S.F., Li, Z.L., Chen, H.L., Santosh, M., Dong, C.W., Yu, X., 2007. Permian bimodal dyke of Tarim Basin, NW China: geochemical characteristics and tectonic implications. Gondwana Research 12 (1–2), 113–120.
Yu, X., 2009. Magma Evolution and Deep Geological Processes of Early Permian Tarim Large Igneous Province. Doctoral Dissertation of Zhejiang University,pp. 1–130, (in Chinese with English abstract).
Yu, X., Chen, H.L., Yang, S.F., Li, Z.L., Wang, Q.H., Lin, X.B., Xu, Y., Luo, J.C., 2009. Geochemical features of Permian basalts in Tarim Basin and compared with Emeishan LIP. Acta Petrologica Sinica 25 (6), 1492–1498 (in Chinese with English abstract).
Yu, J.C., Mo, X.X., Dong, G.C., Yu, X.H., Xing, F.C., Li, Y., Huang, X.K., 2011. Felsic volcanic rocks from northern Tarim, NW China: zircon U–Pb dating and geochemical characteristics. Acta Petrologica Sinica 27 (7), 2184–2194 (in Chinese with English abstract).
Yu, X., Yang, S.F., Chen, H.L., Chen, Z.Q., Li, Z.L., Batt, G.E., Li, Y.Q., 2011. Permian flood basalts from the Tarim Basin, Northwest China: SHRIMP zircon U–Pb dating and geochemical characteristics. Gondwana Research 20 (2–3), 485–497.
Yu, J.C., Mo, X.X., Yu, X.H., Dong, G.C., Fu, Q., Xing, F.C., 2012. Geochemical characteristics and petrogenesis of Permian basaltic rocks in Keping area, Western Tarim basin: a record of plume–lithosphere interaction. Journal of Earth Science 23 (4), 442–454.
Zeng, Q., Yang, J., Zhang, Z., Liu, J., Duan, X., 2014. Petrogenesis of the Yangchang Mo-bearing granite in the Xilamulun metallogenic belt, NE China: geochemistry, zircon U–Pb ages and Sr–Nd–Pb isotopes. Geological Journal 49 (1), 1–14.
Zhang, S.B., Ni, Y.N., Gong, F.H., Lu, H.N., Huang, Z.B., Lin, H.L., et al., 2003. A Guide to the Stratigraphic Investigation on the Periphery of the Tarim Basin. Petroleum Industry Press, Beijing, pp. 1–280 (in Chinese).
Zhang, C.L., Li, X.H., Li, Z.X., Ye, H.M., Li, C.N., 2008. A Permian layered intrusive complex in the Western Tarim Block, Northwestern China:Product of a ca. 275-Ma mantle plume? Journal of Geology 116 (3), 269–287.
Zhang, H.A., Li, Y.J., Wu, G.Y., Su, W., Qian, Y.X., Meng, Q.L., Cai, X.Y., Han, L.J., Zhao, Y., Liu, Y.L., 2009. Isotopic geochronology of Permian igneous rocks in the Tarim Basin. Chinese Journal of Geology 44 (1), 137–158 (in Chinese with English abstract).
Zhang, C.L., Xu, Y.G., Li, Z.X., Wang, H.Y., Ye, H.M., 2010. Diverse Permian magmatism in the Tarim Block, NW China: genetically linked to the Permian Tarim mantle plume? Lithos 119 (3–4), 537–552.
Zhang, Y.T., Liu, J.Q., Guo, Z.F., 2010. Permian basaltic rocks in the Tarim basin, NW China: implications for plume–lithosphere interaction. Gondwana Research 18 (4), 596–610.
Zhang, D.Y., Zhou, T.F., Yuan, F., Fan, Y., Liu, S., Du, H.X., 2010c. LA-ICPMS U–Pb ages, Hf isotope characteristics of zircons from basalts in the Kupukuziman Formation, Keping area, Tarim Basin. Acta Petrologica Sinica 26 (3), 963–974 (in Chinese with English abstract).
Zhang, D.Y., Zhou, T.F., Yuan, F., Jowitt, S.M., Fan, Y., Liu, S., 2012. Source, evolution and emplacement of Permian Tarim Basalts: evidence from U–Pb dating, Sr–Nd–Pb–Hf isotope systematics and whole rock geochemistry of basalts from the Keping area, Xinjiang Uygur Autonomous region, northwest China. Journal of Asian Earth Sciences 49, 175–190.
Zhang, D.Y., Zhang, Z.C., Santosh, M., Cheng, Z.G., Huang, H., Kang, J.L., 2013. Perovskite and baddeleyite from kimberlitic intrusions in the Tarim large igneous province signal the onset of an end-Carboniferous mantle plume. Earth and Planetary Science Letters 361, 238–248.
Zhang, C.L., Zou, H.B., Li, H.K., Wang, H.Y., 2013. Tectonic framework and evolution of the Tarim Block in NW China. Gondwana Research 23, 1306–1315.
Zhong, H., Zhu, W.G., Song, X.Y., He, D.F., 2007. SHRIMP U–Pb zircon geochronology, geochemistry, and Nd–Sr isotopic study of contrasting granites in the Emeishan large igneous province, SW China. Chemical Geology 236, 112–133.
Zhong, H., Zhu, W.G., Hu, R.Z., Xie, L.W., He, D.F., Liu, F., Chu, Z.Y., 2009. Zircon U–Pb age and Sr–Nd–Hf isotope geochemistry of the Panzhihua A-type syenitic intrusion in the Emeishan large igneous province, southwest China and implications for growth of juvenile crust. Lithos 110, 109–128.
Zhong, H., Campbell, I.H., Zhu, W.G., Allen, C.M., Hu, R.Z., Xie, L.W., He, D.F., 2011. Timing and source constraints on the relationship between mafic and felsic intrusions in the Emeishan large igneous province. Geochimica et Cosmochimica Acta 75 (5), 1374–1395.
Zhou, M.F., Zhao, J.H., Qi, L., Su, W., Hu, R., 2006. Zircon U–Pb geochronology and elemental and Sr-Nd isotope geochemistry of Permian mafic rocks in the Funing area, SW China. Contributions to Mineralogy and Petrology 151 (1), 1–19.
Zhou, M.F., Zhao, J.H., Jiang, C.Y., Gao, J.F., Wang, W., Yang, S.H., 2009. OIB-like, heterogeneous mantle sources of Permian basaltic magmatism in the western Tarim Basin, NW China: implications for a possible Permian large igneous province. Lithos 113 (3–4), 583–594.
Zindler, A., Hart, S., 1986. Chemical geodynamics. Annual Review of Earth and Planetary Sciences 14, 493–571.
Zou, S.Y., Li, Z.L., Ren, Z.Y., Li, Y.Q., Yang, S.F., Chen, H.L., Song, B., Yu, X., 2013. U–Pb dating and Hf isotopic compositions of detrital zircons from Permian sedimentary rocks in Keping area of Tarim Basin, Xinjiang, China: constraints on geological evolution of Tarim Block. Acta Petrologica Sinica 29 (10), 3369–3388 (in Chinese with English abstract).